International Journal of Biological Macromolecules

Investigating the inhibition of xanthine oxidase by five catechins: Kinetic studies, spectroscopy, molecular docking, and dynamics simulations

Graphical abstract

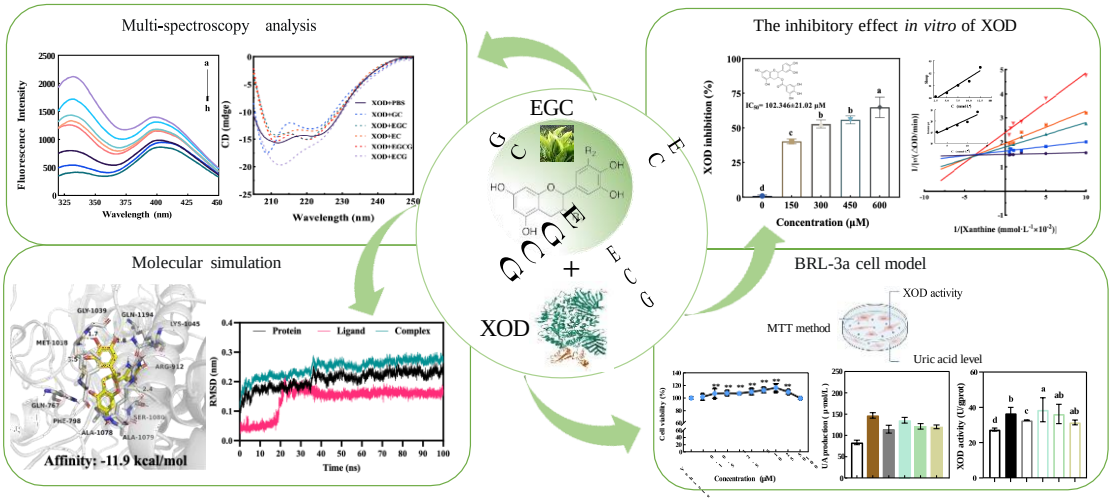

Highlights

- ✓ EGCG and ECG exhibited stronger XOD inhibitory activity compared to GC, EGC, and EC
- ✓ Five catechins showed mixed inhibition activity against XOD
- ✓ 3,4,5-Trihydroxybenzoic acid structure at C_3 of EGCG and ECG enhanced their affinity activity with XOD
- ✓ Inhibitory mechanisms of five catechins on XOD were elucidated
- ✓ EGCG and ECG showed better performance for declining uric acid levels in BRL-3a cells
- ✓ Structure-activity relationships of catechins on inhibiting XOD were analyzed

Revised manuscript (clean version) Click here to view linked References

Investigating the inhibition of xanthine oxidase by five catechins: Kinetic studies, spectroscopy, molecular docking, and dynamics simulations

Xiaoze Liu[1*], Wen Zhang[1*], Jingwen Chen[1], Ruihui Fu[1], Xue Lin[1,2], Shaobo Zhou[3], Lu Wang[1,2#]

1. School of Food Science and Engineering, Hainan University, Haikou 570228, P. R. China;

2. Key Laboratory of Food Nutrition and Functional Food of Hainan Province, Hainan University, Haikou 570228, P. R. China;

3. School of Science, Faculty of Engineering and Science, University of Greenwich, Central Avenue, Chatham ME4 4TB, UK

* These authors contributed equally to this article

Corresponding authors:

Lu Wang, E-mail: lwang@hainanu.edu.cn; Tel: +86-0898-13367470969; Fax: +86-0898-13367470969; People's Avenue, Meilan District, Haikou, China

Abbreviation

GC (gallocatechin), EGC (epigallocatechin), EC (epicatechin), ECG (epicatechin gallate), EGCG (epigallocatechin gallate), UA (uric acid), XOD (xanthine oxidase), CD (circular dichroism), RMSD (root mean square deviation), RMSF (root mean square fluctuation)

Abstract

Catechins compounds from tea have demonstrated significant inhibitory effects on xanthine oxidase (XOD). However, the precise inhibitory mechanisms of the main catechins on XOD remain to be fully elucidated. This study explored the inhibition mechanisms and binding characteristics of five catechins (GC, EGC, EC, EGCG, and ECG) on XOD through a combination of inhibition kinetics, multi-spectroscopy analysis, molecular docking, and dynamics simulations. Among the catechins, EGCG and ECG exhibited the most potent inhibitory activities against XOD. All five catechins were found to exhibit mixed inhibition, affecting the hydrophobic groups and secondary structure of XOD predominantly through hydrophobic interactions and hydrogen bonding. Molecular dynamics simulations revealed that a 3,4,5-trihydroxybenzoic acid moiety at C_3 position significantly enhances the binding affinity of EGCG and ECG to XOD. Additionally, the decrease of β-sheet and random coil induced by EGCG and ECG was found to be crucial for enhancing inhibitory activity of XOD. *In vitro* cell experiments showed that EGCG and ECG significantly reduced high uric acid levels of BRL-3A cell. This study elucidates the inhibitory mechanisms of catechins on XOD, paving the way for their application as XOD inhibitors to combat hyperuricemia.

Keywords: catechins; xanthine oxidase; molecular docking; molecular dynamics simulation; BRL-3a cells

1. Introduction

Hyperuricemia is a common metabolic disorder characterized by elevated levels of uric acid in the blood [1]. Hyperuricemia represents a significant public health issue, impacting a vast segment of the global population. Recent epidemiological studies indicate a rising prevalence of hyperuricemia worldwide. This condition is strongly linked to several health complications, such as gout, kidney stones, and cardiovascular diseases [2, 3]. Several factors contribute to the development of hyperuricemia, including dietary habits, genetic predisposition, obesity, and certain medical conditions such as hypertension and diabetes [1, 4]. The increasing prevalence of hyperuricemia underscores the urgent need for innovative therapeutic strategies.

Xanthine oxidase (XOD) is a crucial enzyme in purine metabolism, responsible for converting hypoxanthine to xanthine and then to uric acid, playing a pivotal role in this biochemical pathway [5]. Hyperuricemia arises from excessive XOD activity, disrupting the balance between uric acid production and its elimination, leading to elevated uric acid levels [6, 7]. Inhibiting xanthine oxidase (XOD) activity is recognized as an effective method for managing hyperuricemia, aimed at lowering blood uric acid levels [8]. Clinically, XOD inhibitors are commonly prescribed for treating hyperuricemia and related disorders, such as gout. Nevertheless, certain synthetic XOD inhibitors (such as allopurinol and febuxostat) have been linked to significant side effects, including hepatotoxicity, allergic reactions, and adverse drug interactions [9]. This has spurred interest in exploring natural compounds as safer alternatives for XOD inhibition.

Catechins, naturally occurring polyphenols abundant in tea, have been the focus of extensive research for their XOD inhibitory potential [10]. These compounds, also found in various dietary sources like vegetables and fruits [11]. Catechins have two benzene rings (A and B rings) and a dihydropyran heterocycle (C ring). The two benzene rings are linked by a dihydropyran heterocycle to form the basic structure of catechins. Catechins are classified into different types based on the structures and spatial conformations of their carbon rings, including gallocatechin (GC), epigallocatechin (EGC), epicatechin (EC), epicatechin gallate (ECG), and epigallocatechin gallate (EGCG). While these catechins also show antioxidant, anti-tumor, anti-inflammatory, and antiviral properties, their therapeutic potential as XOD inhibitors is particularly noteworthy [12]. Among these, EGCG has been particularly well-documented for its XOD inhibitory activities *in vitro* and *in vivo* [13]. For instance, Ali et al. put forwarded that there is a significant difference in the inhibitory activity of different catechin monomers (catechin and EGCG) in green tea against XOD, and that this difference may be due to structural differences [14]. Additionally, Zhang et al. demonstrated that EGCG and gallocatechin gallate (GCG) act as effective natural XOD inhibitors by reducing uric acid levels, stabilizing the XOD structure, and blocking substrate entry through hydrogen bonding and van der Waals interactions [15]. Despite their promising inhibitory effects, the exact mechanisms by which different catechins interact with XOD, leading to varying inhibitory activities, remain unclear. This underscores the importance of exploring the structure-activity relationships among

84 catechins to fully understand their binding mechanisms and optimize their use as XOD
85 inhibitors [16].

86 This study evaluates the XOD inhibitory effects of five primary catechins derived
87 from tea through in vitro inhibition kinetics. It further investigates the binding
88 mechanisms of these catechins to XOD using multi-spectroscopy analysis, molecular
89 docking, and molecular dynamics simulations. Additionally, the study assesses the uric
90 acid-lowering effects of these catechins in xanthine-induced BRL-3a cells. A
91 comparative analysis explores the structure-activity relationship of the five catechins
92 concerning their XOD inhibitory activity. The findings offer a comprehensive
93 understanding of how catechins inhibit XOD and suggest the potential of tea-derived
94 catechins as natural XOD inhibitors for preventing hyperuricemia.

95 **2. Materials and methods**

96 **2.1. Materials**

97 Xanthine oxidase (XOD, from bovine milk, ≥ 0.1 units/mg protein, X4875), xanthine
98 (purity: ≥ 99%, X104264) and allopurinol (purity: ≥ 99%, A8003) were sourced from
99 Sigma-Aldrich (Shanghai, China). Phosphate buffer (pH = 6.8) was obtained from
100 Solarbio (Beijing, China). Gallocatechin (GC), epigallocatechin (EGC), epicatechin
101 (EC), epicatechin gallate (ECG), and epigallocatechin gallate (EGCG) was obtained
102 from Herbal source Biotechnology Co., LTD (Nanjing, China). The uric acid assay kit
103 (C012-2-1) and XOD assay kit (A002-1-1) were provided by Nanjing Jiancheng
104 Bioengineering Institute (Nanjing, China). BRL-3a cells were acquired from the Procell

Life Science & Technology Co., Ltd (Wuhan, China). All other reagents were of analytical grade.

2.2. XOD inhibitory ability *in vitro*

The *in vitro* XOD inhibitory activity was assessed following a modified version of the method described by Yan et al. [17]. Briefly, a reaction mixture containing 0.1 $U \cdot mL^{-1}$ XOD (25 μL) and various concentrations of the five catechins (25 μL) was incubated for 10 minutes at 37°C. Subsequently, xanthine solution (50 μL, 1 mmol/L) was added, mixed well, and the absorbance was measured at 295 nm. Allopurinol served as a positive control, while phosphate-buffered saline (PBS) acted as a blank control. The inhibition rates were calculated using equation (1), and the IC50 values for the catechins were determined with SPSS Statistics (version 19.0).

$$\text{Inhibition rate } (\%) = (1 - \frac{A}{B}) \times 100\% \quad (1)$$

where A represents the absorbance of the inhibitor group; B represents the absorbance of the group without inhibitor.

2.3. Inhibitory kinetics analysis

The inhibition kinetics of catechins against XOD were analyzed using a modified Lineweaver-Burk curve approach, as described by Yan et al. [17]. Briefly, varying concentrations of the five catechins were combined with a 0.01 U/mL XOD solution and incubated at 37°C for 5 minutes before the addition of xanthine. Absorbance at 290 nm was measured every 10 seconds using a UV-visible spectrophotometer. The type of inhibition and kinetic constants were determined using equations (2-4):

$$\frac{1}{v} = \frac{K}{V_{Vmax}}\left(1 + \frac{[I]}{K_i}\right)\frac{1}{[S]} + \frac{1}{V_{max}}\left(1 + \frac{[I]}{\alpha K_i}\right) \quad (2)$$

127 $$Sloop = \frac{K_m}{V_{max}} + \frac{K_m[I]}{V_{max}K_i} \quad (3)$$

128 $$Y_{intercept} = \frac{1}{V_{ma}}(1 + \frac{[I]}{K_{is}}) \quad (4)$$
x

129 In the equation, K_m represents the Michaelis-Menten constant; v and V_{max} denote the
130 reaction rate and maximum reaction rate, respectively; K_i and K_{is} represent the free and
131 binding constants, respectively; [S] and [I] represent the concentrations of the substrate
132 xanthine and catechins, respectively.

133 **2.4. Fluorescence spectra measurement**

134 Fluorescence spectroscopy analysis was conducted using an F-4500 fluorescence
135 spectrophotometer (Hitachi, Tokyo, Japan), equipped with a 450 W xenon lamp and a
136 constant temperature water bath [18]. In this process, 2.5 mL of XOD solution (0.05
137 U/mL) was placed into a quartz test tube. Subsequently, varying concentrations of the
138 five catechins were introduced, mixed, and incubated at temperatures of 298, 303, and
139 310 K for 10 minutes. The fluorescence spectra were then measured using settings of a
140 scanning wavelength range of 290~500 nm, an excitation wavelength of 280 nm, and
141 excitation and emission bandwidths set to 5 nm each. A phosphoric acid buffer (pH 7.4)
142 served as a blank to adjust for fluorescence background. To elucidate the quenching
143 mechanism of the catechins on XO, analysis was performed employing the Stern-
144 Volmer equation (5) and (6):

145 $$\frac{F_0}{F} = 1 + K_{sv}[Q] = 1 + K_q \tau_0[Q] \quad (5)$$

146 $$\log\frac{F_0 - F}{F} = \log K + n\log[Q] \quad (6)$$

147 where F_0 and F represent the fluorescence intensities of XOD in the absence and
148 presence of catechins, respectively; K_q, τ_0 mean the quenching rate constant and

average lifetime, respectively; [Q] is the account of catechins, and K_{SV} is the Stern-Volmer quenching constant; n is the number of binding sites.

2.5. Synchronous fluorescence spectra

Synchronous fluorescence spectra were performed following the procedure of Zhao et al. Synchronous fluorescence spectra of XOD and XOD-Catechins were tested in the wavelength range of 250-350 nm. The emission wavelength interval values ($\Delta\lambda$) were set to 15 and 60 nm, respectively. The synchronous fluorescence burst ratio (RSFQ) of tyrosine and tryptophan residues was calculated using Eq. (7).

$$\mathrm{RSFQ} = (1 - (\mathrm{F}/\mathrm{F}_0)) \times 100\% \quad (7)$$

where F_0 and F denote the fluorescence intensity of XO in the absence of catechins and containing catechins, respectively.

2.6. Circular dichroism (CD) measurements

Circular dichroism spectra of the catechins-XOD complexes were obtained using a J-815 CD spectrometer (JASCO, Japan) [19]. An XOD solution (0.02 U/mL) and catechin solutions at varying concentrations were prepared in phosphate-buffered saline (PBS, pH 7.4) and mixed to form the complexes. PBS served as the blank, and different concentrations of catechins were measured separately to eliminate their impact on the spectra. The CD spectra were recorded in 1 mm quartz cuvettes at room temperature under a nitrogen atmosphere. Scans covered the wavelength range from 200 nm to 260 nm, with settings adjusted to a scanning speed of 200 nm/min, a step resolution and bandwidth of 1 nm, a response time of 0.5 seconds, and a sensitivity of 20 millidegrees. The quantification of enzyme secondary structure components was performed using the

CONTIN algorithm available at the DichroWeb website (https://dichroweb.cryst.bbk.ac.uk/html/home.shtml).

2.7. Molecular docking

Molecular docking analyses of catechins and XOD were conducted using AutoDock (version 4.2.6). Catechin structures were initially designed using ChemDraw 11.0 (Cambridge Soft Corporation, Cambridge, Massachusetts, USA). These structures were then converted to mol2 format with Open Babel GUI and subsequently optimized using the Tripos force field energy minimization principle. AutoDockTools was utilized to prepare the small molecules, including the optimization of protonation states and hydrogen orientations. The 3D crystal structure of XOD from bovine milk (PDB ID: 1FIQ) was retrieved from the Protein Data Bank (http://www.rcsb.org/pdb) and prepared for docking by removing water molecules, adding polar hydrogens, and assigning Kollman united atom charges. The protein was also subjected to energy minimization using Gromacs software (version 2022) to relieve any steric clashes.

The docking grid box was centered on the active site of XOD, particularly focusing on the MoS hydrophobic cavity [20]. The grid was set to dimensions of 40Å × 40Å × 40Å with a grid spacing of 0.375Å, ensuring that the entire active site was covered. The Lamarckian genetic algorithm (LGA) was employed as the docking algorithm, ensuring a thorough exploration of the conformational space. Three independent docking runs were performed, generating 30 different conformations for each catechin. The best binding conformation was selected based on the lowest binding energy and the consistency of the docking poses across multiple runs.

2.8. Molecular dynamics simulations

Molecular dynamics simulations were performed using Gromacs software (version 2022). GAFF force fields were applied to the catechins using AmberTools22, while Gaussian 16W was employed for hydrogenation and RESP potential calculations, which were incorporated into the molecular dynamics system's topology file. The simulations were performed at a constant temperature of 300 K and atmospheric pressure (1 Bar), using the amber99sb-ildn force field and the TIP3P water model. The system's total charge was neutralized with Na^+ ions The simulation process began with energy minimization using the steepest descent method, followed by equilibration phases: 100,000 steps in the NVT ensemble and the NPT ensemble with a coupling constant of 0.1 ns, each lasting 100 ns. Finally, a comprehensive molecular dynamics simulation was conducted over 5,000,000,000 steps with a 2 fs timestep, totaling 100 ns.

2.9. Evaluation of uric acid-lowering activity by BRL-3a cells

2.8.1. Cell culture

BRL-3a cells was obtained from the Procell Life Science & Technology Co., Ltd (Wuhan, China) and cultured in 25 cm^2 flasks in a medium containing 1% penicillin/streptomycin, 10% fetal bovine serum, and 89% MEM in an incubator at 37℃ and 5% CO_2. The culture medium was changed every 1−2 day, and cells were subculture every 2 days.

2.8.2. MTT method

Following the method described by Xiao et al. [21], the MTT assay was utilized to assess the impact of five catechins on BRL-3a cell viability, aiming to establish a safe dosage for intake. Initially, BRL-3a cells, upon reaching 80-90% confluence, were detached using 0.25% trypsin and plated in a 96-well plate at a density of 2×10^4 cells per well. After allowing 12 hours of cell attachment, the existing supernatant was removed. he catechins were first dissolved in DMSO to create stock solutions, which were then further diluted to desired concentrations with the culture medium. Subsequently, each well received the medium enriched with 1% catechin solutions and was incubated in a CO_2 incubator. After 48 hours, the supernatant was removed and replaced with MEN mixed with 15% MTT solution (1 mg/mL) in each well. The plate was then placed back in the incubator. After 4 hours, the supernatant was discarded and 150 μL of DMSO was added to each well. After 10 minutes of incubation, the absorbance was measured at 490 nm. The cell viability was calculated using the following equation (8):

$$\text{Cell viability } (\%) = \frac{OD_2 - OD_1}{OD_1 - OD_0} \times 100 \quad (8)$$

In the equation, OD_0 represents the background value of the plate, OD_1 represents the absorbance value of the blank control, and OD_2 represents the absorbance value of the sample treatment group.

2.8.3. Determination of UA level and XOD activity in BRL 3A cells

UA level and XOD activity in BRL 3A cells were determined following the protocol outlined by Liu et al. [22]. BRL 3A cells in the logarithmic growth phase were enzymatically dissociated and resuspended in complete growth medium, then seeded

at a density of 5×10^5 cells per well in a plate. After 16 hours of incubation, the supernatant in each well was discarded, and the cells were washed twice with PBS. Subsequently, the cells were treated with 1 mM xanthine along with varying concentrations of catechins (GC, EGC, EC, EGCG, and ECG), while allopurinol was employed as a positive control. Following a 48-hour incubation period, both the cells and their supernatant were harvested. The cell supernatant underwent centrifugation at 1000 × g for 5 minutes, after which uric acid levels were quantified using a uric acid assay kit (Nanjing Jiancheng, C012-2-1). Additionally, the cell pellet was lysed using cell lysis buffer containing 1 mM PMSF, followed by centrifugation at 12000 × g for 10 minutes to isolate cellular proteins. The protein concentration was determined using the BCA Protein Concentration Assay kit (Beyotime). Finally, the XOD activity in the cells was measured using an XOD activity assay kit (Nanjing Jiancheng, A002-1-1).

2.10. Statistical analysis

The experiments were repeated three times. The results were expressed as mean ± standard deviation (SD). Data were analyzed by using SPSS version 18.0 software (SPSS Inc., Chicago, IL, USA) and Graphpad Prism 5 (GraphPad Software Inc., San Diego, CA). One-way ANOVA was used to detect the differences of the data. *p*-value < 0.05 was indicated as significant.

3. Results and discussion

3.1. Inhibitory activity of five catechins on XOD

The inhibitory activities of five catechins (GC, EGC, EC, EGCG, and ECG) against XOD were compared in this study. As shown in Fig. 1A-F, a dose-dependent relationship was observed between the concentrations of the five catechins and their inhibitory effects on XOD. The IC_{50} value of the positive drug, AP, was determined to be 2.634 ± 0.286 μM. Notably, the IC_{50} values for GC, EGC, EC, EGCG, and ECG were 5.663 ± 0.42 mM, 4.655 ± 0.25 mM, 3.265 ± 1.59 mM, 102.346 ± 21.02 μM, and 152.200 ± 6.95 μM, respectively. Interestingly, EGC exhibited significantly higher XOD inhibitory activity compared to GC ($p < 0.05$), despite being stereoisomers. While the number of hydroxyl groups typically influences XOD inhibition, our study revealed unexpected results [16]. Specifically, EC, lacking the -OH group at position C3 in B ring, showed significantly better XOD inhibitory activity than GC and EGC ($p < 0.05$). Similarly, consistent results were observed in the comparison between EGCG and ECG. EGCG exhibited higher XOD inhibitory activity than ECG ($p < 0.05$), which had an additional -OH group at position C3'. Furthermore, to investigate the effect of the galloyl moieties (3,4,5-trihydroxybenzoic acid) structure at position C3 on XOD inhibition, we compared the XOD inhibitory activities of EC and ECG. The results demonstrated that ECG had significantly higher XOD inhibitory activity than EC due to the addition of 3,4,5-trihydroxybenzoic acid at position C3 ($p < 0.05$). Cao et al. reported that galloyl moieties are essential for the anti-amylase activity of catechins, therefore, based on structural advantages, 3,4,5-trihydroxybenzoic acid may be responsible for the higher inhibitory activity of EGCG and ECG [23]. To sum up, EGCG and ECG have stronger inhibitory activity on XOD at low concentrations

compared to GC, EGC and EC. It is speculated that the introduction of 3,4,5-trihydroxybenzoic acid structure increased the inhibitory activity of XOD.

3.2. Inhibitory kinetic analysis of five catechins on XOD

The Lineweaver-Burk method was employed to characterize the inhibition types of catechins on XOD. As shown in the Fig. 2A-E, the slope of the lines increased proportionally with the concentration of catechins. Notably, the Y-intercept ($1/V_{max}$) and X-intercept ($1/K_m$) of the Lineweaver-Burk curve exhibited significant changes with increasing catechin concentration. Furthermore, all regression lines intersected in the second quadrant in each plot, indicating that all five catechins inhibit XOD in a mixed mode, which is consistent with the report of Zhang et al. [15]. Using nonlinear regression analysis and the Michaelis-Menten model, we determined K_m and V_{max} values, as presented in Table 1. The result showed that the presence of catechins led to an increase in K_m value and a decrease in V_{max} [24]. As a result, the catechins occupied the active site of XOD, preventing catalytic substrates like xanthine from binding to the enzyme, thereby reducing the production of excessive catalytic products, thereby increasing K_m value. This means that a higher substrate concentration is required to reach half the maximum reaction rate in the presence of catechins. On the other hand, catechins decreased the catalytic activity of the enzyme, resulting in a decrease of V_{max} [24]. The inhibition constants (K_i) and XOD-substrate complex (K_{is}) were calculated by eqs. (2) and (3), respectively. In addition, the K_{is} values of GC (K_i = 33.140 μM, K_{is} = 188.600 μM), EGC (K_i = 34.100 μM, K_{is} = 180.900 μM), EC (K_i = 52.400 μM, K_{is} = 153.000 μM), EGCG (K_i = 0.023 μM, K_{is} = 0.084 μM) and ECG (K_i = 0.028 μM, K_{is} =

0.070 μM) were significantly higher than their K_i values, indicating that the binding ability of catechins to XOD was stronger than that of substrates to XOD (Table 1). In summary, five catechins reversibly inhibited the catalytic activity of XOD in a mixed-type mode.

3.3. Fluorescence quenching analysis

To gain insights into the binding mechanisms between the five catechins and XOD, fluorescence quenching experiments were conducted on XOD in both the presence and absence of catechins. As shown in Fig. 3A1-E1, XOD has two distinct fluorescence emission peaks near 328 nm and 398 nm. The maximum fluorescence emission peak of XOD was shifted due to the addition of different concentrations of catechins. Therefore, the fluorescence intensity under the maximum fluorescence emission peak was taken as F_0 and F for calculation. Phenylalanine (Phe) and tryptophan (Try) constitute the primary hydrophobic amino acids in XOD [25]. Notably, Try serves as the principal endogenous fluorescence source of XOD and exhibits sensitivity to alterations in the microenvironment [17]. This suggests that the Try of XOD are located in the hydrophobic region of the enzyme's active site [26]. Likewise, with increasing concentrations of catechins, the fluorescence intensity of XOD progressively diminishes, suggesting that the presence of the five catechins can engage with the hydrophobic amino acids of XOD and induce alterations in the enzyme's spatial conformation. Drawing insights from the Stern-Volmer curves of XOD (Fig. 3A2-E2 and Fig. 3A3-E3), the quenching reactions of the five catechins with XOD at different temperatures show that K_{sv} decreases with increasing temperature, indicating that the

fluorescence quenching mechanism of the five catechins on XOD is a single type of static quenching [27] (Table 2). Among them, ECG-XOD has the highest K_{sv}, indicating the most stable complex system [28]. Hence, it can be deduced that stable complexes are formed between the catechins and XOD during the fluorescence quenching process. Additionally, the stability of these complexes decreases as the temperature of the reaction system rises. The quenching indices of the fluorescence quenching reaction of five catechins with XOD were further analyzed, as depicted in Table 2. Among the fluorescence quenching reactions of the five catechins with XOD, the K_{sv} values of the EGCG-XOD and ECG-XOD complexes are notably higher. Consequently, these complexes exhibit greater stability compared to other catechins-XOD complexes. The K_q value of the fluorescence quenching reaction of five catechins with XOD is greater than the maximum dispersive collisional quenching rate constant of the quencher and the biomolecule (2.0×10^{10} $L \cdot mol^{-1} \cdot s^{-1}$), i.e., it is in accordance with the reaction condition of static quenching [29]. K_a as a denote the association constant of the quencher-protein receptor system, and the K_a can be calculated by fitting a linear curve of $(F_0\text{-}F)/F$ versus the inverse of the quencher concentration [Q] (Fig. 3K-O). Here, we observed that K_a of the five catechin-XOD complexes was inversely proportional to temperature. It is shown that as the temperature increases, the more unstable the catechins-XOD system becomes.

In addition, when the quencher undergoes a static quenching reaction with the protein, i.e., an equivalent binding site is generated when small molecules with protein [30]. The n values for the quenching reactions of five catechins with XOD are all

approximately equal to 1, indicating the existence of a binding site for five catechins to form a complex with XOD under static quenching. Comparison of the correlation coefficients (R^2) of the three quenching coefficients, K_{sv}, and K_a, indicates a high degree of reasonableness of the reaction equation and the hypothesis analyses above.

3.4. Thermodynamic analysis of catechins binded with XOD

Thermodynamic parameters can represent the interaction forces in the catechins-XOD system, including hydrogen bonding, hydrophobic interactions, van der Waals forces, and electrostatic interactions. The Gibbs free energy change (ΔG), enthalpy change (ΔH), and entropy change (ΔS) were calculated by Van't Hoff equation (9) and (10) [31]:

$$\mathrm{Log}K_a = \frac{\Delta H}{2.303RT} + \frac{\Delta S}{2.303R} \quad (9)$$

$$\Delta G = \Delta H - T\Delta S \quad (10)$$

where R (gas constant) is 8.314 J/mol·K, and the absolute temperatures (T) are 298, 304, and 310 K, respectively. The thermodynamic parameters of these catechins binded with XOD are shown in Table 2. The results suggest consistency in the binding reactions occurring within the independent systems of the five catechins and XOD. The positive values of ΔG suggest that the interaction between catechins and XOD is non-spontaneous. Smaller values of ΔG indicate more stable binding. Notably, the ΔG of GC with XOD was lowest at 298 K, followed by ECG. Moreover, the negative values of ΔH and ΔS indicate that the binding process is primarily driven by van der Waals forces and hydrogen bonding [31].

3.5. Analysis of synchronous fluorescence spectra

The synchronous fluorescence spectra of XOD induced by catechins are shown in Fig .S1. The intensity of XOD decreased significantly with increasing concentrations of catechins, which was consistent with the fluorescence quenching results, further validating the quenching of endogenous fluorescence of XOD by the five catechins. For GC, EGC and ECG, the maximum emission wavelengths of Tyr and Trp were not significantly shifted at 290 nm and 280 nm, respectively (Fig. S2A-B). However, the synchronous fluorescence spectra ($\Delta\lambda$ = 15 nm) of EC and EGCG for XOD showed a slight redshift from 289 to 291 nm and 288 to 292 nm, respectively, which is consistent with the study of Zhao et al [32]. This suggests that the addition of EC and EGCG resulted in an increase in polarity around Tyr, leading to a decrease in XOD hydrophobicity. However, the five catechins did not cause a significant shift in the synchronous fluorescence spectra of XOD in Trp ($\Delta\lambda$ = 60 nm). The results suggest that the five catechins can bind to both Tyr and Trp of XOD, causing a change in the hydrophobicity of XOD and thus inhibiting the activity.

The effects of catechins on Tyr and Trp were further understood by calculating the ratio of synchronous fluorescence quenching (RSFQ) of residues Tyr and Try, and the results are shown in Fig. S1C. For ECG, the RSFQ value of Trp was significantly higher than that of Tyr, suggesting that Trp may contribute better to the fluorescence burst effect of XOD. And the RSFQ values of GC, EGC, EC and EGCG at Trp approximated those at Tyr. The above results suggest that the contribution of Trp and Tyr to the fluorescence burst effect seems to be the same in other catechins except ECG, which may be located at almost the same distance from both residues when

interacting with XOD. Previous studies have suggested that this is because the molecular microenvironment around the active XOD binding site is altered by the addition of EGCG, which ultimately leads to a conformational change of XOD, in agreement with our results [32].

3.6. Circular dichroism spectra

Circular dichroism (CD) spectroscopy is employed to detect alterations in protein secondary structure. The CD spectra of XOD in the presence of the five catechins are illustrated in Fig. 4A. Notably, XOD displays two negative bands at 210 nm and 220 nm in the UV CD spectrum, which are characteristic features of α-helix structure [33]. This suggests that the α-helix structure of XOD undergoes changes upon the addition of the five catechins. Furthermore, a negative absorption peak emerges at 216 nm, which is indicative of β-sheet structure [34]. It can be seen that the five catechins, by altering the α-helix and β-sheet structures of XOD, enhance the rigidity of the protein, making it difficult for the active site of XOD to form, thereby reducing the effective binding of substrates with XOD. Among the five catechins, ECG induces more significant changes in the CD spectra of XOD than the other compounds. The secondary structure content of the enzyme was determined using the CONTIN program, as shown in Fig. 4B. Upon the inclusion of the five catechins in the reaction system, alterations are observed in the α-helix, β-sheet, β-turn, and random structures of XOD. Notably, the percentage of α-helix structure in XOD increases from 6.65% to 7.05%, 5.70%, 7.05%, 9.10%, and 11.95% with the addition of GC, EGC, EC, EGCG, and ECG, respectively. However, EGC diminishes the α-helix content of XOD. With the

411 exception of EGC, the other catechins decrease the *β*-sheet structure of XOD.
412 Specifically, there is a reduction from 40.15% to 37.40% (GC), 37.40% (EC), 37.35%
413 (EGCG), and 38.25% (ECG), respectively. It is noteworthy that, among the catechins
414 studied, ECG exhibits the most pronounced effect in augmenting the *β*-turn and
415 diminishing the content of random coil structure. This alteration influences the
416 originally flexible structure of XOD. Comparable trends in inducing changes in
417 secondary structure by EGCG and ECG have been reported in other studies pertaining
418 to XOD inhibition [15]. In conclusion, the five catechins promote the unfolding of
419 peptide chains and rearrangement of the secondary structure in XOD. However, the
420 alteration of the secondary structure by each catechin varies may be one of the reasons
421 for their differences in XOD inhibitory activity.

422 **3.7. Molecular docking**

423 Further insight into the binding mode between the five catechins and XOD was gained
424 through molecular docking. The optimal docking conformations of the five catechins
425 and AP with XOD are depicted in Fig. 5A-F. Similar to the *in vitro* enzyme inhibition,
426 EGCG and ECG exhibited similar affinity ability on XOD (-11.9 kcal/mol), which were
427 stronger than GC (-8.9 kcal/mol), EGC (-9.2 kcal/mol) and EC (-9.3 kcal/mol). The
428 XOD active site is multi-channeled and the catalytic center is located in a hydrophobic
429 crevice [35]. The five catechins demonstrate the ability to effectively penetrate the
430 active cavity containing the molybdenum sulfur (MoS) and securely anchor within the
431 hydrophobic cavity of XOD, maintaining a consistent conformation. Also, the result of
432 AP's docking in agreement with Pan et al. [20]. We observed that AP occupies the active

site as well. However, limited by the molecular docking algorithm, the binding free energy of AP is much lower than that of catechins (-6.7 kcal/mol). Catechins are flavonoids composed of three rings: the A-ring (with two hydroxyl groups), the B-ring (which varies in hydroxyl group placement and affects protein binding), and the C-ring (a heterocyclic ring connecting A and B that determines catechin's stereochemistry) [36]. Within this arrangement, the A and C rings of the catechins are positioned inside the cavity, while the B ring extends outward. As these phenolic compounds dock within the XOD active pocket, they become ensconced within the hydrophobic cavity containing MoS, characterized by a lower dielectric constant. This configuration enhances the interaction between the small molecules and the catalytic groups [19]. Therefore, the hydrophobic microenvironment favors the binding of five catechins to XOD. Hydrogen bonds play a crucial role in ligand-protein interactions [37]. By observing the binding mode between five catechins and XOD, multiple hydrogen bonds were found between the ligands and the receptor. GC forms hydrogen bonds with GLN-1194, SER-1080, SER-1082, and THR-1083 of XOD, with bond lengths of 2.0 Å, 2.2 Å, 2.8 Å, and 2.2 Å, respectively (Fig. 5A). Similarly to EGC, GLY-799 and MET-1038 are crucial residues facilitating the binding of EGC and EC to XOD (Fig. 5B and C). Additionally, EGC establishes two hydrogen bonds with THR-1083. The planar structure of flavonoid compounds offers an advantage for XOD inhibition. ALA-1078, situated within the active XOD cavity, is predisposed to forming π-π conjugation with the A ring of catechins [20]. Therefore, this serves as compelling evidence for the effective binding of the five catechins to XOD. As shown in Fig. 5D and E, EGCG and ECG

exhibit similar binding modes. GLN-1194 and SER-1080 emerge as crucial residues for the binding of EGCG and ECG to XOD, respectively. All catechins exhibit enhanced π-π conjugation with GLY-1039 owing to the presence of the aromatic ring A. Furthermore, the 3,4,5-trihydroxybenzoic structure of EGCG and ECG is anchored deep in the pocket, thus helping the small molecules to increase spatial hindrance. Additionally, you are in agreement with previous studies that AP forms hydrogen bond binding between AP and XOD multiple key amino acids such as GLU-802, ARG-880, ALA-1079, THR-1010 (Fig. 5F). This binding mode is favorable for stable binding of the compounds in the pocket, thereby blocking the entry of purine substrates [24].

3.8. Molecular dynamics simulation

The influence of the five catechins on the dynamic stability and conformational changes of XOD was assessed through molecular dynamics simulation. The stability of each complex system was evaluated using the root-mean-square deviation (RMSD). As illustrated in Fig. 6A-E, all five catechins-XOD systems achieved equilibrium after 10 nanoseconds, with the Root Mean Square Deviation (RMSD) values leveling off at approximately 0.2 to 0.3 nm. The RMSD values for the catechins-XOD complexes were higher than those observed for XOD in isolation, suggesting that XOD experiences significant conformational changes when interacting with the catechins. Interestingly, RMSD analysis revealed distinct behavior among the catechin monomers. The GC, EGC, and EC monomers exhibited minimal fluctuations, with RMSD values consistently around 0.1 nm, indicating stable binding and minor conformational impact on XOD. In contrast, the EGCG and ECG monomers showed increased RMSD values

ranging from 0.1 to 0.2 nm after 20 ns, suggesting that these catechins engaged in more dynamic interactions with XOD. It is easy to find that the RMSDs of XOD-catechins complexes are all increased by about 0.1 nm compared to XOD. This implies that the fluctuation effect of catechins themselves had an impact on the initial conformation of XOD. At the 100 ns, the RMSD of XOD-catechins were 0.27 nm (XOD-GC), 0.30 nm (XOD-EGC), 0.30 nm (XOD-EC), 0.26 nm (XOD-EGCG), and 0.24 nm (XOD-ECG), respectively. This indicates that XOD-EGCG and XOD-ECG have better stability. These dynamic interactions likely enhanced the flexibility of XOD, leading to altered enzyme activity [24]. Apparently, more hydrogen bonds were formed between EGCG and ECG and XOD, which contributed to the stability of the complex (Fig. 6F).

The influence of five catechins on the fluctuation of XOD amino acid residues was represented by the Root Mean Square Fluctuation (RMSF). As shown in Fig. S2A-E, under identical simulation conditions, the five catechins displayed both similarities in their effects on RMSF values of XOD amino acid residues across five specific regions. These regions encompass the α-helix, β-sheets, and random coil structures at locations 1 (570-590), 2 (740-755), 3 (1105-1130), as well as the pocket region of site 4 (1200-1250) and the flexible side chains rich in random coil structures of site 5 (1270-1290). Therefore, this implies that the modification of XOD by catechins is localised and targeted to modify the α-helix, β-sheets, and random coil structures of XOD, similar to the study by Pan et al [20]. Also consistent with the CD results is that different catechins influence the flexible structure of XOD by affecting different secondary structure regions of XOD and thus the flexible structure of XOD. The difference is that the

interaction of GC with XOD influenced the dynamics of sites 1, 3, 4, and 5. EGC and EC both amplified the movements of sites 1 and 2. Furthermore, EC specifically affected the fluctuations of amino acids within the pocket region, whereas EGC targeted the flexible side chains featuring random coil structures of XOD. Notably, EGCG uniquely intensified the motion at site 5 compared to the other catechins. Lower average RMSF values indicate that a particular amino acid residue exhibits stability in the dynamic state of the protein [38]. In contrast, the modification of EGCG did not cause fluctuations in more amino acid sites of XOD. This implies that XOD-EGCG is more stable than other XOD-catechins.

The radius of gyration (Rg) is utilized to assess the compactness of protein structures. As shown in Fig. S2F, the Rg of the EGCG and ECG-XOD systems remained around 2.80 nm, and both were higher than that of the other catechins-XOD system. This indicates that the binding of EGCG and ECG induced protein folding or unique conformational changes.

3.9. Effects of catechins on lowering uric acid and inhibiting XOD activity in BRL-3a cells

Employing the MTT assay, this study explored the influence of five different catechins on the viability of BRL-3A cells. BRL-3A cells were exposed to various concentrations of the five catechins for a period of 48 hours, after which the rates of cell proliferation were assessed, as depicted in Fig. 7A1-E1. Within a concentration range of 0.1 to 25 μM, there was a direct correlation between the concentration of catechins and the survival rate of BRL-3A cells. Specifically, at concentrations up to 25 μM for EGCG

and ECG, an increase in catechin concentration led to a corresponding increase in cell survival rates. Beyond this threshold, elevations to 50 and 100 μM did not significantly impact the survival rates of BRL-3A cells. Consequently, catechin concentrations up to 100 μM are deemed to be non-toxic to BRL-3A cells.

BRL-3A cells were treated with xanthine for 48 hours to create a model of high uric acid levels. As shown in Fig. 7A2-E2, uric acid (UA) levels in the model group were significantly elevated compared to the normal control (NC) group ($p < 0.05$). The positive control group, treated with allopurinol (AP), exhibited a marked reduction in UA content compared to the model group ($p < 0.05$). Treatment of the BRL-3A cells with different concentrations of catechins resulted in variable effects on UA levels. At a concentration of 100 μM, EGC, GC, and ECG significantly lowered UA levels ($p < 0.05$), whereas EC did not exhibit a significant impact at any tested concentration. Notably, EGCG was effective in reducing UA levels at both 50 μM and 100 μM ($p < 0.05$), highlighting its potential to mitigate high uric acid levels induced by xanthine in BRL-3A cells. These findings corroborate previous research on the urate-lowering properties of EGCG [13].

The inhibition of XOD is crucial in limiting excessive uric acid production. Therefore, the effects of the five catechins on XOD activity in BRL 3A cells were further determined. As shown in Fig. 7A3-E3, the group treated with allopurinol demonstrated a significant decrease in xanthine oxidase (XOD) activity within BRL-3A cells ($p < 0.01$). Regrettably, with the exception of EGCG and ECG, none of the other catechins, across various concentrations, meaningfully reduced XOD activity in

these cells. In summary, at a cellular level, catechins, with the exception of EC, were observed to substantially lower uric acid (UA) levels at a concentration of 100 μM. Nonetheless, given that the reduction in UA levels is not solely dependent on diminished XOD enzyme activity but also on multiple other factors, further research is essential to elucidate the mechanisms behind the urate-lowering effects of these catechins.

3.10. Structure-activity relationships of catechins on inhibiting XOD

In this preliminary investigation of the structure-activity relationships, the inhibitory effects of five catechins on xanthine oxidase (XOD) were assessed in vitro by determining their half-maximal inhibitory concentration (IC_{50}) values. Studies have indicated that the hydroxyl groups (-OH) located at the C5 and C7 positions on the catechins play a crucial role in the inhibition of XOD [39]. Significant variances were observed in the inhibitory potency among the catechin isomers, with GC exhibiting markedly higher inhibition compared to EGC, and EGCG outperforming ECG, suggesting that a non-planar configuration of the aromatic ring B, as well as substitutions at the C3 position, are more conducive to XOD inhibition. Notably, EGCG's inhibitory effect was found to be nearly 30-fold greater than that of EC, leading to the conclusion that the presence of a galloyl ester group at the C3 position significantly enhances catechins' inhibitory capabilities. Additionally, EGCG's structural configuration, particularly the stereo-orientation of the aromatic ring B and the C3 substituent, indicates a strategic advantage, proposing that the planarity of ring B and its C3 substituent may play a crucial role in mitigating XOD activity. It was also

established that all five catechins function as mixed inhibitors against XOD, capable of binding to both the enzyme itself and the enzyme-substrate complex. The binding of catechins affected the microenvironment of Trp and Tyr as well as the secondary structure of the enzyme, thereby influencing its catalytic activity and hydrophobicity. In contrast to previous reports, the thermodynamic calculations showed that the binding between the five catechins and XOD was non-spontaneous, and their binding was driven by van der Waals forces and hydrogen bonding [15]. This may be due to the presence of a small amount of bovine serum albumin in XOD, and the components of the serum albumin may introduce additional molecules and particles, increasing the particle number in the system and thus altering the degree of disorder and thermodynamic changes of the system [40]. Molecular docking and kinetic simulations revealed that hydrogen bonding and π-π conjugation contribute to the strong binding between catechins and XOD. For catechins, and the π-π conjugation system formed by the aromatic ring A are considered essential for XOD inhibition [39]. Additionally, EGCG and ECG exhibited higher affinity due to the substituent at C3, the galloyl ester. Zhang et al. posited that the adaptable stereochemistry of EGCG might contribute to its stable interaction with XOD, a finding corroborated by our investigation [15]. Moreover, we assessed the urate-lowering efficacy of five catechins within a BRL-3A cell model exhibiting elevated uric acid levels, induced by xanthine exposure. At elevated concentrations (100 μM), all catechins markedly diminished intracellular uric acid concentrations, displaying a dose-responsive relationship. Nonetheless, aside from EGCG and ECG, the remaining catechins failed to significantly impact XOD activity

within the cells. This discrepancy likely stems from structural variations among the catechins, indicating that their urate-reducing effects extend beyond direct XOD inhibition. Given that catechins exhibit antioxidant and anti-inflammatory attributes, and considering the link between uric acid synthesis and oxidative stress alongside inflammatory processes, it's plausible that catechins mitigate uric acid levels through attenuating oxidative stress and inflammation. Additionally, these results were consistent with the reports of Li et al [13], who suggest that the galloyl ester group at the C3 position is crucial for inhibiting XOD activity within cells. However, the study is limited in that it does not extend these comparisons to *in vivo* models. Specifically, the differential effects of the five catechins on hyperuricemia improvement and the underlying mechanisms were not explored in animal models or clinical studies. Future research should aim to address these gaps by conducting in vivo studies to provide a more comprehensive understanding of the therapeutic potential of these catechins.

4. Conclusions

This study provides a comprehensive analysis of the inhibitory mechanisms exerted by five catechins (GC, EGC, EC, EGCG, and ECG) on xanthine oxidase (XOD) activity. EGCG and ECG demonstrated superior inhibitory effects on XOD in vitro compared to GC, EGC, and EC, functioning through a mixed-type inhibition mode. These catechins effectively quenched XOD's intrinsic fluorescence via a static quenching mechanism, indicating significant alterations in the enzyme's hydrophobic regions and secondary structure—largely driven by hydrophobic interactions and hydrogen bonding. Notably, EGCG and ECG, characterized by a 3,4,5-trihydroxybenzoic acid moiety at

609 the C3 position, displayed enhanced binding affinity towards XOD relative to the other
610 catechins. Molecular docking studies suggested that inhibition by these catechins
611 occurs through their insertion into the key active catalytic site of XOD, thereby
612 blocking substrate access and inducing structural changes within the enzyme. Moreover,
613 EGCG and ECG decreased the proportion of β-sheet and random coil structures in XOD,
614 correlating with their heightened inhibitory impact. Cellular experiments further
615 confirmed that EGCG and ECG more effectively reduced uric acid levels by
616 suppressing intracellular XOD activity. In summary, the potent inhibitory action of
617 catechins against XOD can be attributed to the presence of a 3,4,5-trihydroxybenzoic
618 acid structure at the C3 position of the catechins. This investigation offers a theoretical
619 foundation for harnessing catechins derived from tea as XOD inhibitors, providing a
620 strategic approach to combat hyperuricemia.

621 **Author Contributions**

622 **Xiaoze Liu** and **Wen Zhang:** Methodology, Investigation, Data analysis, Wrote the
623 original draft; **Jingwen Chen, Ruihui Fu, Shaobo Zhou** and **Xue Lin:** Resources
624 and Investigation, Data analysis and Data curation; **Lu Wang:** Supervision, Funding,
625 Data curation and Reviewing & Editing.

626 **Acknowledgments**

627 The study was supported by the National Natural Science Foundation of China (No.
628 32201991 and No. 32360109), and the Collaborative Innovation Center project of
629 Hainan University, China (No. XTCX2022NYC19).

630 **Conflict of interest**

The authors declare no competing financial interest.

Figure captions

Figure 1. Inhibitory activity of allopurinol (A), GC (B), EGC (C), EC (D), EGCG (E), and ECG (F) on XOD. Significant differences ($p < 0.05$) between treatments are denoted by letters above the corresponding bars in the chart.

Figure 2. Lineweaver-Burk plots for XOD with varying concentrations of catechins. For GC (A), concentrations were 2, 1, 0.5, 0.25, 0.1 mM (lines a→e); for EGC (B), concentrations matched those in (A); for EC (C), concentrations were identical to (A) and (B); for EGCG (D), concentrations were 0.4, 0.2, 0.1, 0.05, 0.025 mM (lines a→e); for ECG (E), concentrations were as in (D). Secondary plots illustrate the intercept and slope versus inhibitor concentrations, respectively. Each data point represents the mean of triplicate measurements.

Figure 3. Fluorescence quenching spectra of XOD in the presence of catechins across different concentrations (A1-E1). For GC, EGC, and EC, concentrations range from 0 to 10 μM (lines a→h), while for EGCG and ECG, concentrations also range from 0 to 10 μM, except ECG extends only up to 5 μM for lines a→h. the Stern-Volmer figure of xanthine oxidase with different concentrations of catechins (GC: A2, A3; EGC: B2, B3; EC: C2, C3; EGC: D2, D3; EGCG: E2, E3; ECG: F2, F3). Temperatures 298, 304, and 310 K are represented, indicating experiments conducted at different Kelvin temperatures. Each point reflects the average of three measurements.

652 **Figure 4.** (A) Circular dichroism (CD) spectra of XOD in the presence and absence of
653 catechins (GC, EGC, EC, EGCG, and ECG). (B) Analysis of XOD's secondary
654 structure content derived from CD spectra, comparing conditions without and with
655 the five catechins.
656 **Figure 5.** Molecular docking outcomes showing the interactions between XOD and
657 each catechin: GC (A), EGC (B), EC (C), EGCG (D), and ECG (E). Binding
658 affinities are quantified as free energy values.
659 **Figure 6.** Root Mean Square Deviation (RMSD) for the GC-XOD (A), EGC-XOD (B),
660 EC-XOD (C), EGCG-XOD (D), and ECG-XOD (E) systems throughout 100 ns
661 molecular dynamics (MD) simulations. Panel (F) illustrates the variation in the
662 number of hydrogen bonds within each of the five catechin-XOD systems over the
663 course of the 100 ns simulation.
664 **Figure 7.** Evaluation of cell viability (A1-E1), uric acid levels (A2-E2), and
665 intracellular XOD activity (A3-E3) in BRL-3A cells following exposure to five
666 catechins: GC (A), EGC (B), EC (C), EGCG (D), and ECG (E), respectively.
667 **Figure S1.** The synchronous fluorescence spectra of XOD and RSFQ in the absence
668 and presence of five catechins GC (1), EGC (2), EC (3), EGCG (4) and ECG (5)
669 at $\Delta\lambda$ = 15 (A) and 60 nm (B). Concentration of GC, EGC, EGCG, ECG= 0, 10,
670 20, 40, 60, 80, 100 μM for curves a → g, respectively; and concentration of EC =
671 0, 1, 2, 4, 6, 8, 10 μM for curves a → g, respectively.
672 **Figure S2.** the Root Mean Square Fluctuation (RMSF) for the GC-XOD (A), EGC-
673 XOD (B), EC-XOD (C), EGCG-XOD (D), and ECG-XOD (E) systems

674 throughout 100 ns molecular dynamics (MD) simulations. Rg (F) illustrates the
675 variation in radius of gyration within each of the five catechin-XOD systems over
676 the course of the 100 ns simulation.
677
678
679

References

[1] S.J. Cheng, L.S. Shan, Z.Y. You, Y. Xia, Y.H. Zhao, H.H. Zhang, Z.Y. Zhao, Dietary patterns, uric acid levels, and hyperuricemia: a systematic review and meta-analysis, Food Funct. 14(17) (2023) 7853-7868.

[2] J.G. Jiang, T.J. Zhang, Y.S. Liu, Q. Chang, Y.H. Zhao, C.J. Guo, Y. Xia, Prevalence of Diabetes in Patients with Hyperuricemia and Gout: A Systematic Review and Meta-analysis, Curr. Diabetes Rep. 23(6) (2023) 103-117.

[3] H. Yanai, H. Adachi, M. Hakoshima, H. Katsuyama, Molecular Biological and Clinical Understanding of the Pathophysiology and Treatments of Hyperuricemia and Its Association with Metabolic Syndrome, Cardiovascular Diseases and Chronic Kidney Disease, Int. J. Mol. Sci. 22(17) (2021) 20.

[4] L. Sun, C.X. Ni, J.X. Zhao, G. Wang, W. Chen, Probiotics, bioactive compounds and dietary patterns for the effective management of hyperuricemia: a review, Crit. Rev. Food Sci. Nutr. (2022) 16.

[5] M. Bortolotti, L. Polito, M.G. Battelli, A. Bolognesi, Xanthine oxidoreductase: One enzyme for multiple physiological tasks, Redox Biol. 41 (2021) 6.

[6] M.G. Battelli, M. Bortolotti, L. Polito, A. Bolognesi, The role of xanthine oxidoreductase and uric acid in metabolic syndrome, Biochimica Et Biophysica Acta-Molecular Basis of Disease 1864(8) (2018) 2557-2565.

[7] M.G. Battelli, M. Bortolotti, L. Polito, A. Bolognesi, Metabolic syndrome and cancer risk: The role of xanthine oxidoreductase, Redox Biol. 21 (2019).

[8] M.A. Becker, H.R. Schumacher, L.R. Espinoza, A.F. Wells, P. MacDonald, E. Lloyd, C. Lademacher, The urate-lowering efficacy and safety of febuxostat in the treatment of the hyperuricemia of gout: the CONFIRMS trial, Arthritis Res. Ther. 12(2) (2010) 12.

[9] S.Z. Zhang, T. Xu, Q.Y. Shi, S.Y. Li, L. Wang, Z.M. An, N. Su, Cardiovascular Safety of Febuxostat and Allopurinol in Hyperuricemic Patients With or Without Gout: A Network Meta-Analysis, Front. Med. 8 (2021) 10.

[10] Y. Chen, L. Luo, S. Hu, R. Gan, L. Zeng, The chemistry, processing, and preclinical anti-hyperuricemia potential of tea: a comprehensive review, Crit. Rev. Food Sci. Nutr. 63(24) (2023) 7065-7090.

[11] P. Ninfali, E. Antonini, A. Frati, E.S. Scarpa, C-Glycosyl Flavonoids from Beta vulgaris Cicla and Betalains from Beta vulgaris rubra: Antioxidant, Anticancer and Antiinflammatory ActivitiesA Review, Phytother. Res. 31(6) (2017) 871-884.

[12] T.Y. Wang, Q. Li, K.S. Bi, Bioactive flavonoids in medicinal plants: Structure, activity and biological fate, Asian J. Pharm. Sci. 13(1) (2018) 12-23.

[13] F. Li, Y. Liu, Y. Xie, Z. Liu, G. Zou, Epigallocatechin gallate reduces uric acid levels by regulating xanthine oxidase activity and uric acid excretion in vitro and in vivo, Annals of Palliative Medicine 2(2) (2020) 1128-1128.

[14] A. Rashidinejad, E.J. Birch, D.W. Everett, Green tea catechins suppress xanthine oxidase activity in dairy products: An improved HPLC analysis, J. Food Compos. Anal. 48 (2016) 120-127.

[15] G.W. Zhang, M. Zhu, Y.J. Liao, D.M. Gong, X. Hu, Action mechanisms of two key xanthine oxidase inhibitors in tea polyphenols and their combined effect with allopurinol, J. Sci. Food Agric. 102(15) (2022) 7195-7208.

[16] H. Xue, M. Xu, D. Gong, G. Zhang, Mechanism of flavonoids inhibiting xanthine oxidase and alleviating hyperuricemia from structure–activity relationship and animal experiments: A review, Food Frontiers 4(4) (2023) 1643-1665.

[17] J.K. Yan, G.W. Zhang, Y.T. Hu, Y.D. Ma, Effect of luteolin on xanthine oxidase: Inhibition kinetics and interaction mechanism merging with docking simulation, Food Chem. 141(4) (2013) 3766-3773.

[18] H.P. Li, M.M. Zhao, G.W. Su, L.Z. Lin, Y. Wang, Effect of Soy Sauce on Serum Uric Acid Levels in Hyperuricemic Rats and Identification of Flazin as a Potent Xanthine Oxidase Inhibitor, Journal of Agricultural and Food Chemistry 64(23) (2016) 4725-4734.

[19] Y.J. Li, X.Y. Kang, Q.Y. Li, C.C. Shi, Y.Y. Lian, E.D. Yuan, M. Zhou, J.Y. Ren, Anti-hyperuricemic peptides derived from bonito hydrolysates based on in vivo hyperuricemic model and in vitro xanthine oxidase inhibitory activity, Peptides 107 (2018) 45-53.

[20] Y. Pan, Z.K. Lu, C.C. Li, R.R. Qi, H. Chang, L. Han, W.W. Han, Molecular Dockings and Molecular Dynamics Simulations Reveal the Potency of Different Inhibitors against Xanthine Oxidase, ACS Omega 6(17) (2021) 11639-11649.

[21] B.P. Xiao, Y.Y. Li, Y.Q. Lin, J.Y. Lin, L.Y. Zhang, D.R. Wu, J. Zeng, J. Li, J.W. Liu, G.L. Li, Eicosapentaenoic acid (EPA) exhibits antioxidant activity via mitochondrial modulation, Food Chem. 373 (2022) 8.

[22] X.Z. Liu, D.R. Wu, J.W. Liu, G.L. Li, Z.X. Zhang, C.X. Chen, L.Y. Zhang, J. Li, Characterization of xanthine oxidase inhibitory activities of phenols from pickled radish with molecular simulation, Food Chem. X 14 (2022) 10.

[23] J. Cao, Y. Zhang, L. Han, S. Zhang, X. Duan, L. Sun, M. Wang, Number of galloyl moieties and molecular flexibility are both important in alpha-amylase inhibition by galloyl-based polyphenols, Food Funct. 11 (2020).

[24] J. Zhao, L. Huang, C. Sun, D. Zhao, H. Tang, Studies on the structure-activity relationship and interaction mechanism of flavonoids and xanthine oxidase through enzyme kinetics, spectroscopy methods and molecular simulations - ScienceDirect, Food Chem. 323(1) (2020) 126807.

[25] Z.-d. Qi, Y. Zhang, F.-L. Liao, Y.-W. Ou-Yang, Y. Liu, X. Yang, Probing the binding of morin to human serum albumin by optical spectroscopy, Journal of pharmaceutical and biomedical analysis 46(4) (2008) 699-706.

[26] D.P. Acharya, L. Sanguansri, M.A. Augustin, Binding of resveratrol with sodium caseinate in aqueous solutions, Food Chem. 141(2) (2013) 1050-1054.

[27] A. Papadopoulou, R.J. Green, R.A. Frazier, Interaction of flavonoids with bovine serum albumin: a fluorescence quenching study, Journal of agricultural and food chemistry 53(1) (2005) 158-63.

[28] Y. Zhang, Q.X. Zhong, Binding between Bixin and Whey Protein at pH 7.4 Studied by Spectroscopy and Isothermal Titration Calorimetry, Journal of Agricultural and Food Chemistry 60(7) (2012) 1880-1886.

[29] S.M. Darwish, S.E. Abu Sharkh, M.M. Abu Teir, S.A. Makharza, M.M. Abu-Hadid, Spectroscopic investigations of pentobarbital interaction with human serum albumin, J. Mol. Struct. 963(2-3) (2010) 122-129.

[30] N. Bijari, Y. Shokoohinia, M.R. Ashrafi-Kooshk, S. Ranjbar, S. Parvaneh, M. Moieni-Arya, R. Khodarahmi, Spectroscopic study of interaction between osthole and human serum albumin: Identification of possible binding site of the compound, J. Lumines. 143 (2013) 328-336.

[31] J.H. Xie, H.X. Cui, Y. Xu, L.H. Xie, W. Chen, Delphinidin-3-O-sambubioside: a novel xanthine oxidase inhibitor identified from natural anthocyanins, Food Qual. Saf. 5 (2021) 10.

[32] J. Zhao, L. Huang, C.Y. Sun, D.S. Zhao, H.J. Tang, Studies on the structure-activity relationship and interaction mechanism of flavonoids and xanthine oxidase through enzyme kinetics, spectroscopy methods and molecular simulations, Food Chem. 323 (2020) 11.

[33] W.H. Gao, N.N. Li, Y.W. Chen, Y.P. Xu, Y.J. Lin, Y.G. Yin, Z.D. Hu, Study of interaction between syringin and human serum albumin by multi-spectroscopic method and atomic force microscopy, J. Mol. Struct. 983(1-3) (2010) 133-140.

[34] Y. Wan, J. Qian, Y.Z. Li, Y.F. Shen, Y.R. Chen, G.M. Fu, M.Y. Xie, Inhibitory mechanism of xanthine oxidase activity by caffeoylquinic acids in vitro, Int. J. Biol. Macromol. 184 (2021) 843-856.

[35] Enroth, Cristofer, Eger, T. Bryan, Crystal structures of bovine milk xanthine dehydrogenase and xanthine oxidase: Structure-based, Proceedings of the National Academy of Sciences of the United States of America (2000).

[36] K.E. Heim, A.R. Tagliaferro, D.J. Bobilya, Flavonoid antioxidants: chemistry, metabolism and structure-activity relationships, The Journal of nutritional biochemistry 13(10) (2002) 572-584.

[37] Y.X. Zheng, W.H. Yang, W.X. Sun, S.G. Chen, D.H. Liu, X.L. Kong, J.H. Tian, X.Q. Ye, Inhibition of porcine pancreatic α-amylase activity by chlorogenic acid, J. Funct. Food. 64 (2020) 7.

[38] Y. Liu, C.G. Han, T. Lu, Y. Liu, H. Chen, C. Yang, Y.B. Tu, Y.F. Li, Investigation of the interaction between Chrysoeriol and xanthine oxidase using computational and in vitro approaches, Int. J. Biol. Macromol. 190 (2021) 463-473.

[39] P. Cos, L. Ying, M. Calomme, J.P. Hu, K. Cimanga, B. Van Poel, L. Pieters, A.J. Vlietinck, D.V. Berghe, Structure-activity relationship and classification of flavonoids as inhibitors of xanthine oxidase and superoxide scavengers, Journal of Natural Products 61(1) (1998) 71-76.

795 [40] J.B. Xiao, F.F. Mao, F. Yang, Y.L. Zhao, C. Zhang, K. Yamamoto, Interaction of dietary
796 polyphenols with bovine milk proteins: Molecular structure-affinity relationship and
797 influencing bioactivity aspects, Mol. Nutr. Food Res. 55(11) (2011) 1637-1645.
798

Figure 1

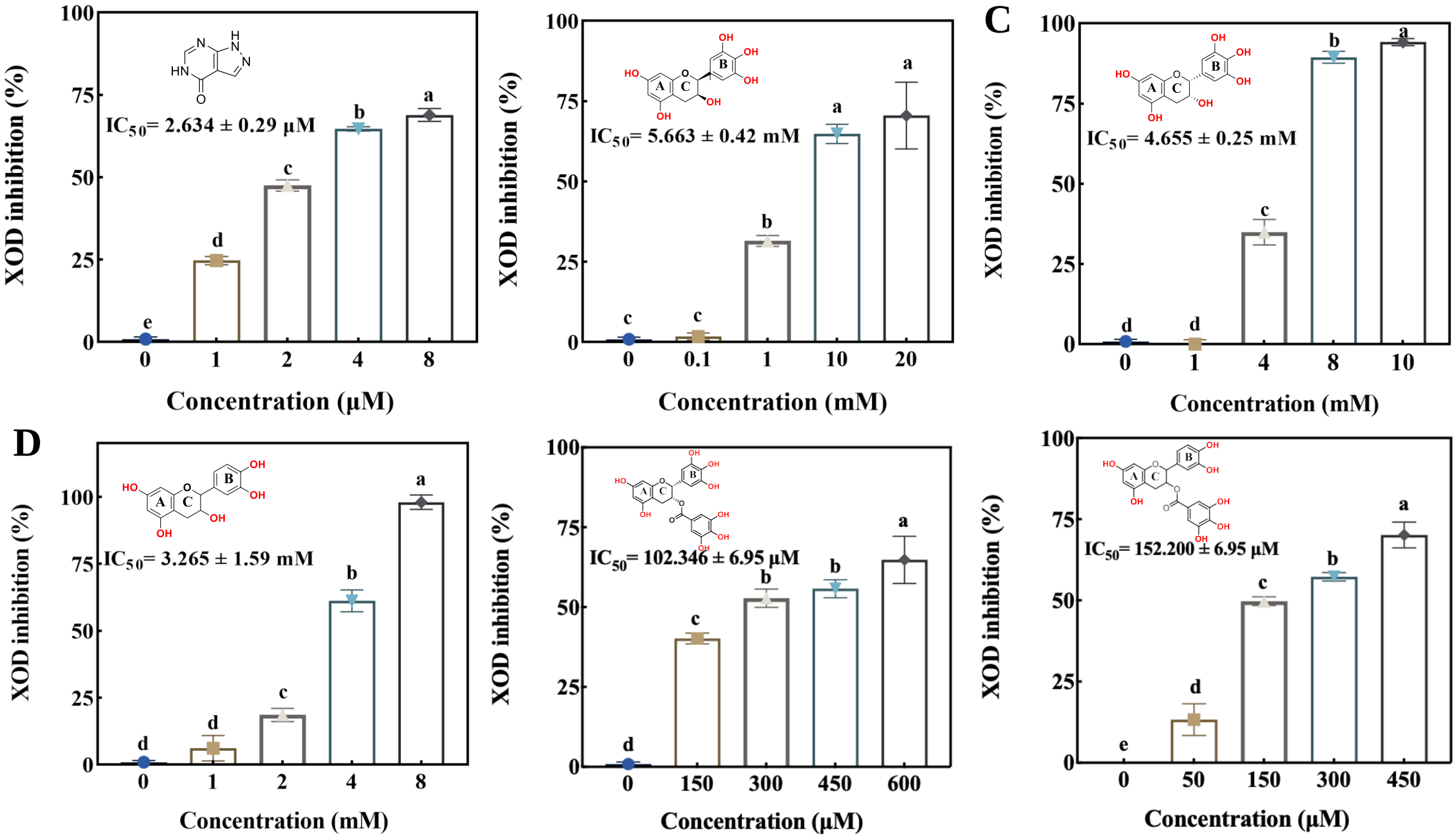
C
D
XOD inhibition (%)
Concentration (μM)
Concentration (mM)
IC50= 2.634 ± 0.29 μM
IC50= 5.663 ± 0.42 mM
IC50= 4.655 ± 0.25 mM
IC50= 3.265 ± 1.59 mM
IC50= 102.346 ± 6.95 μM
IC50= 152.200 ± 6.95 μM

Click here to access/download;Figure;Figure 2.ppt

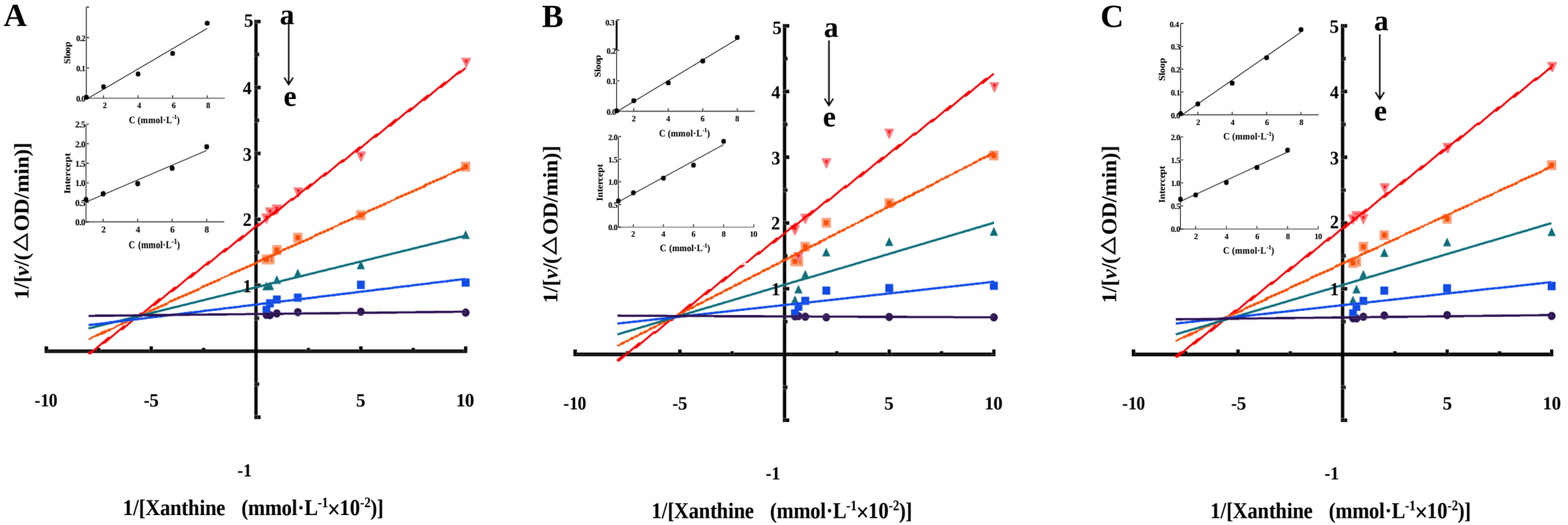

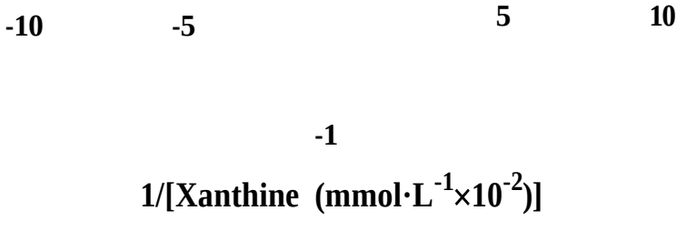
-10
-5
5
10
-1
1/[Xanthine (mmol·L-1×10-2)]

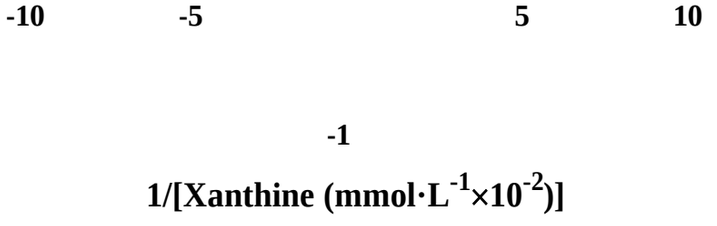
-10
-5
5
10
-1
1/[Xanthine (mmol·L-1×10-2)]

Figure 3
Click here to access/download;Figure;Figure 3.ppt

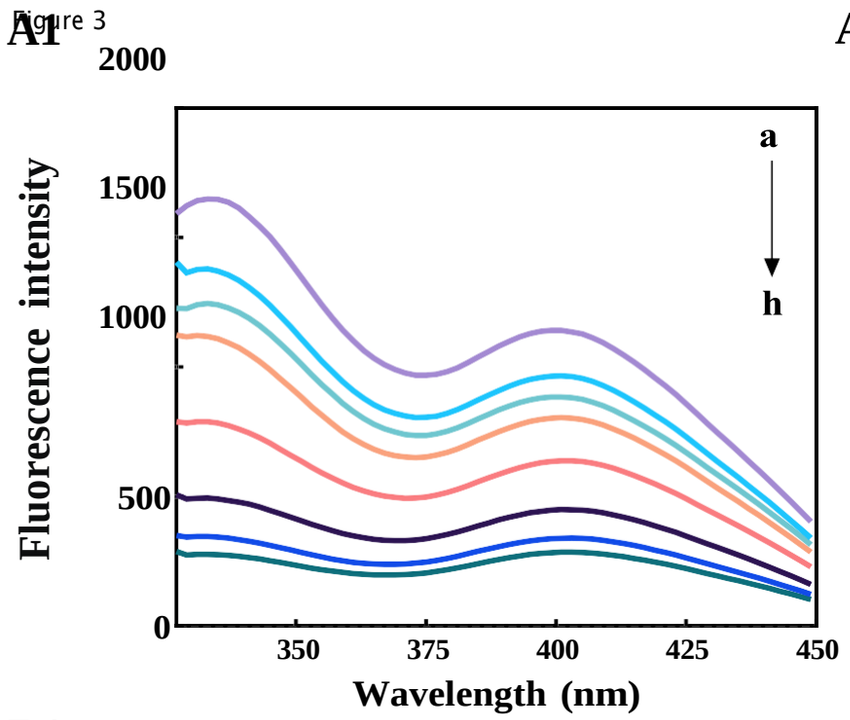

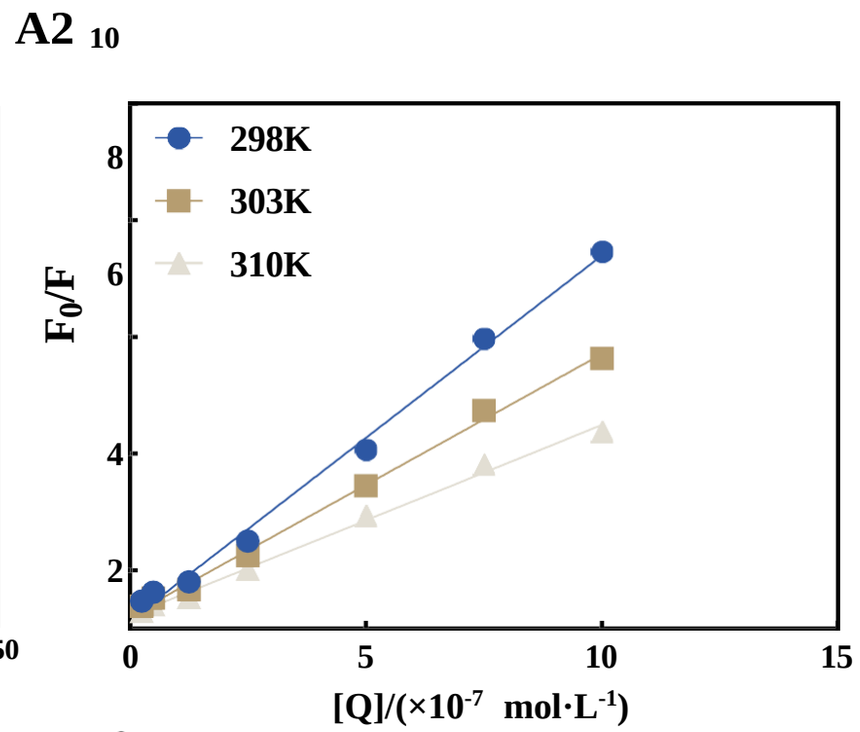

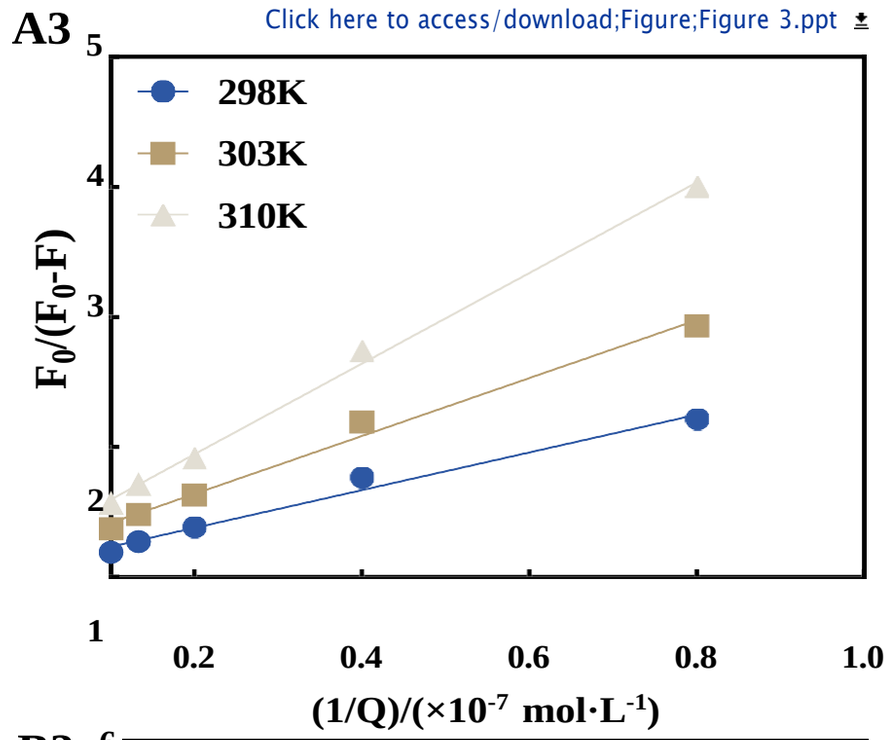

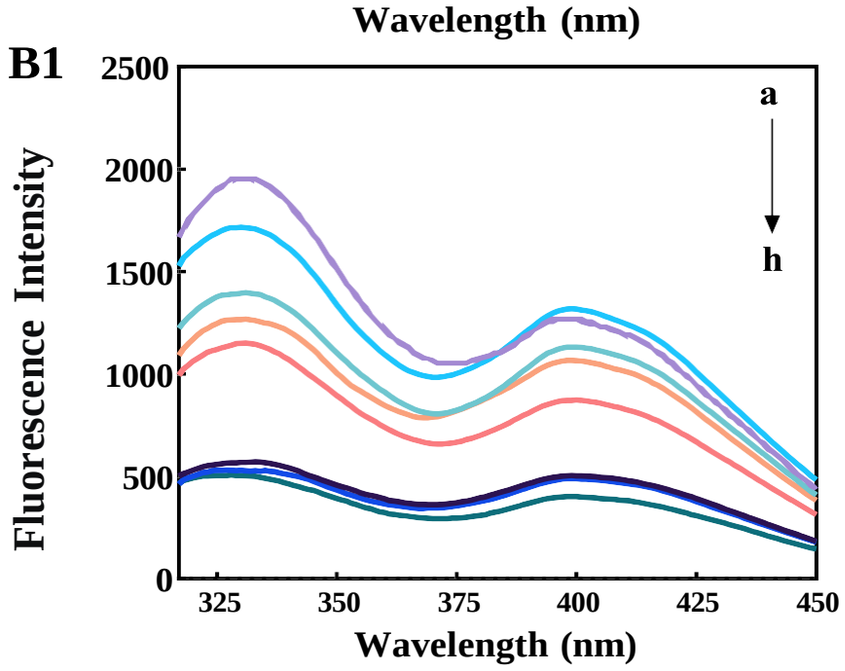

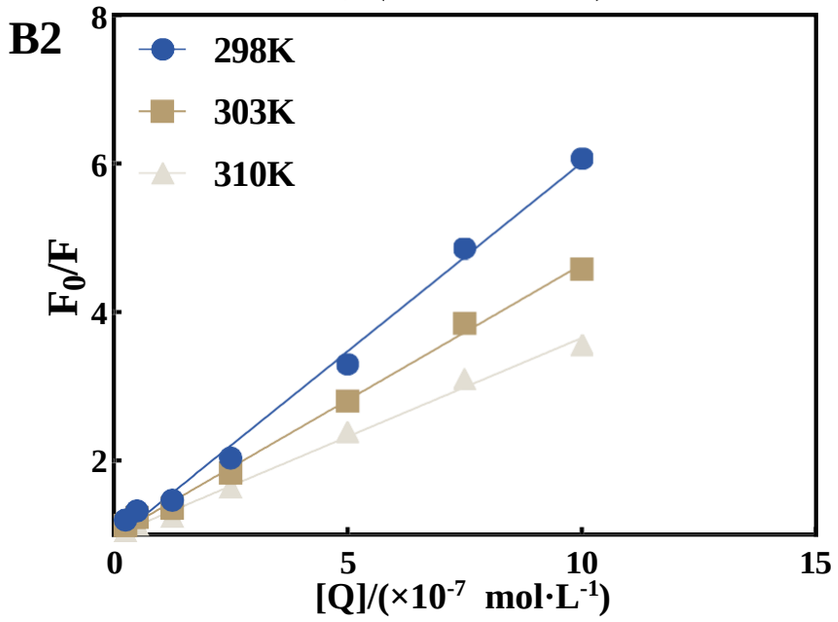

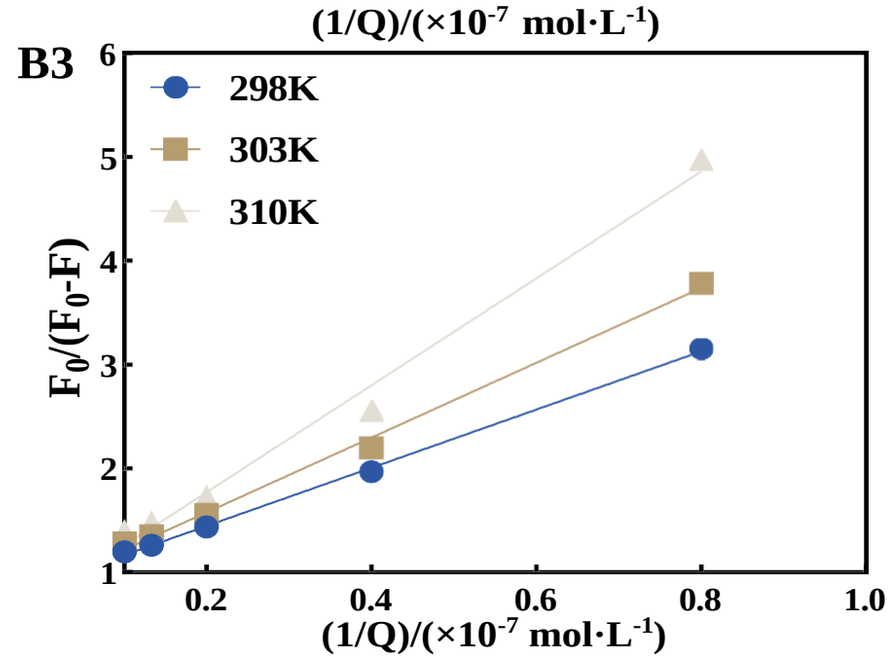

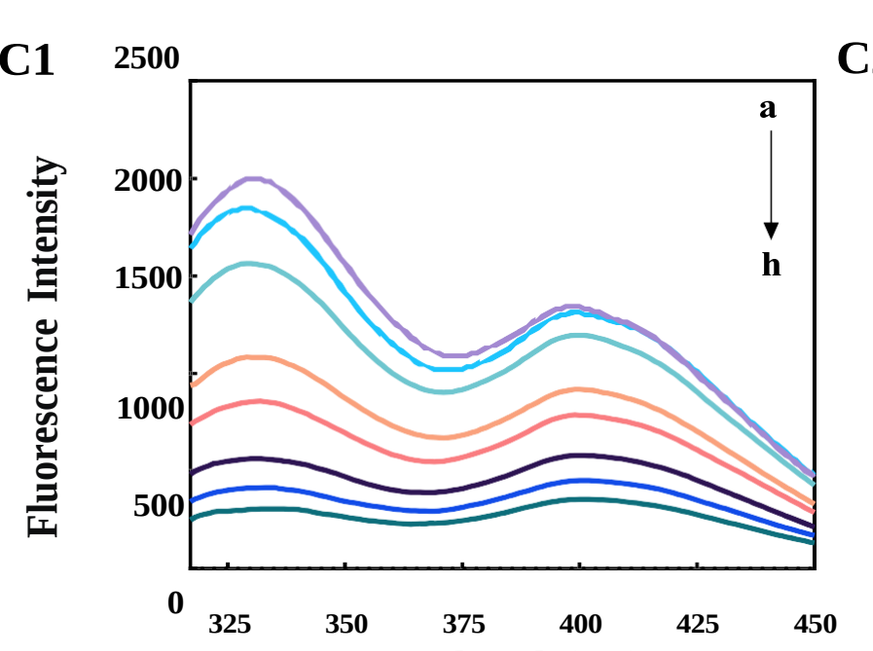

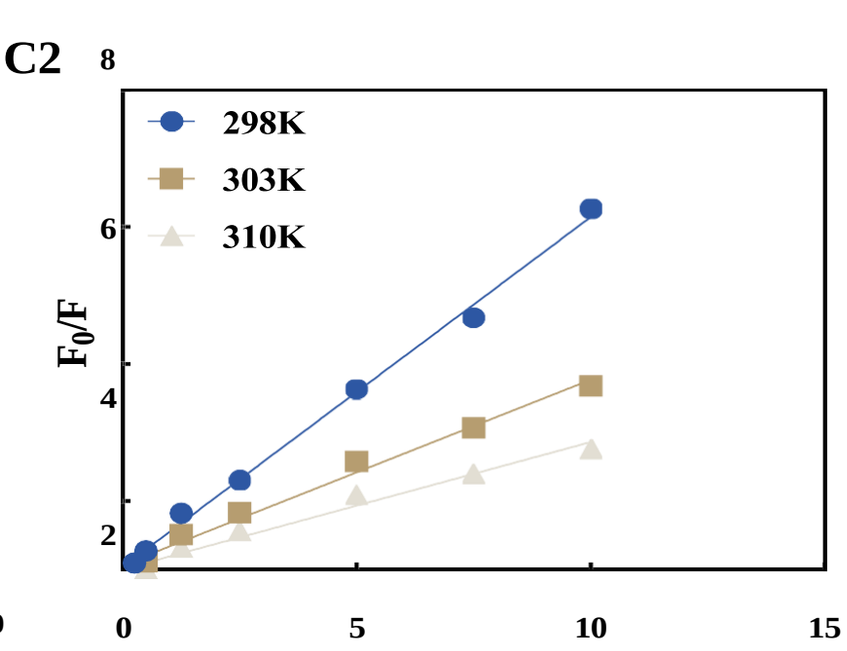

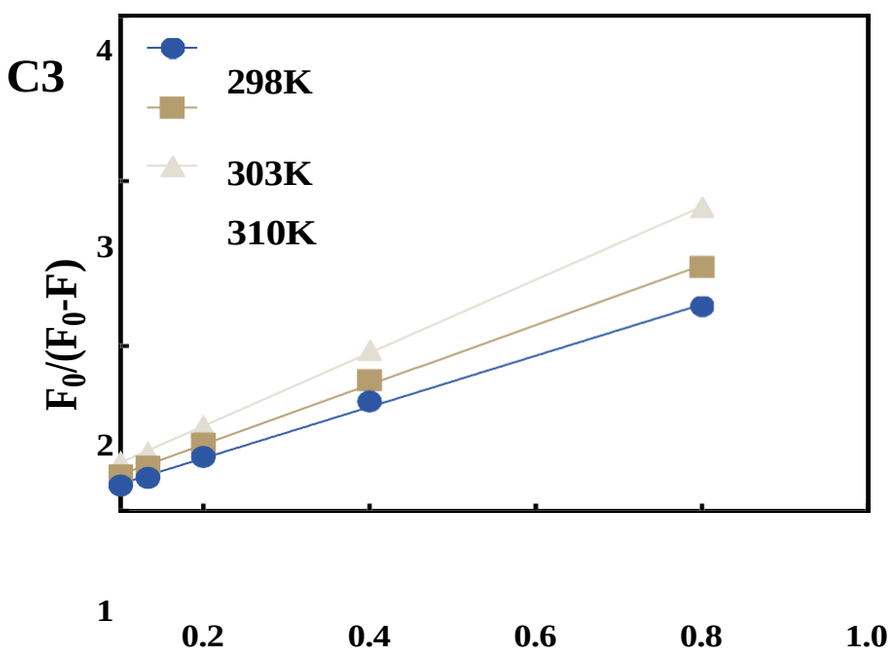

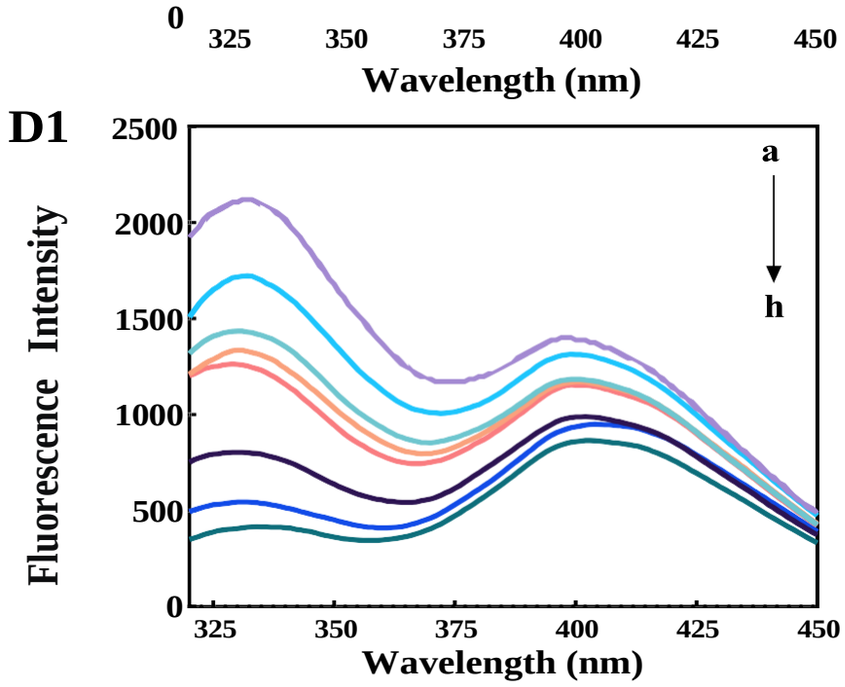

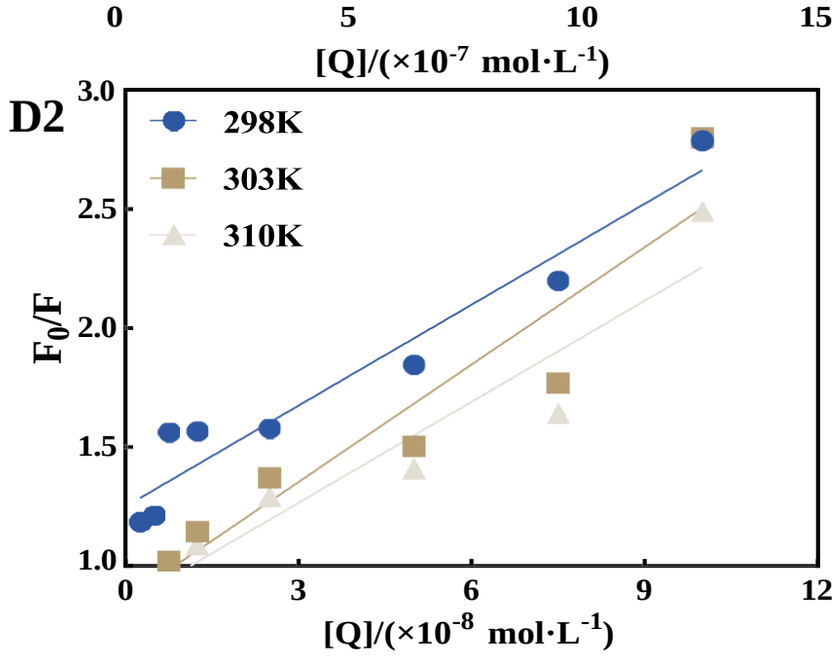

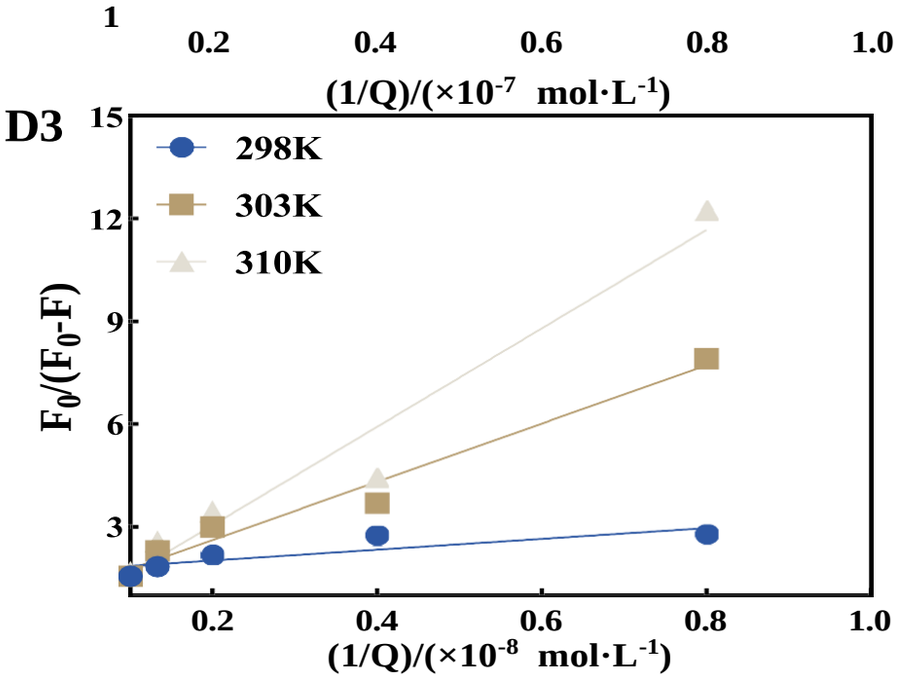

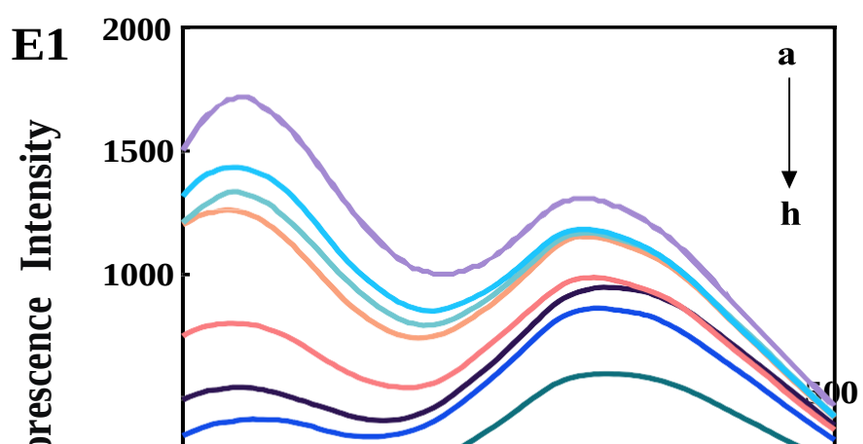

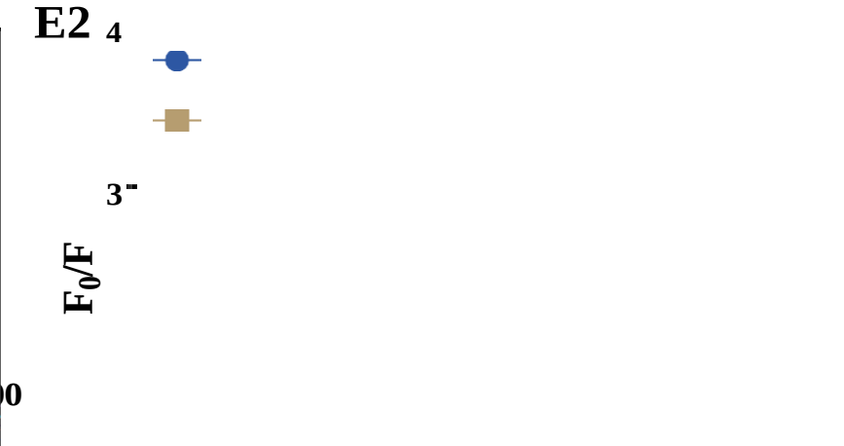

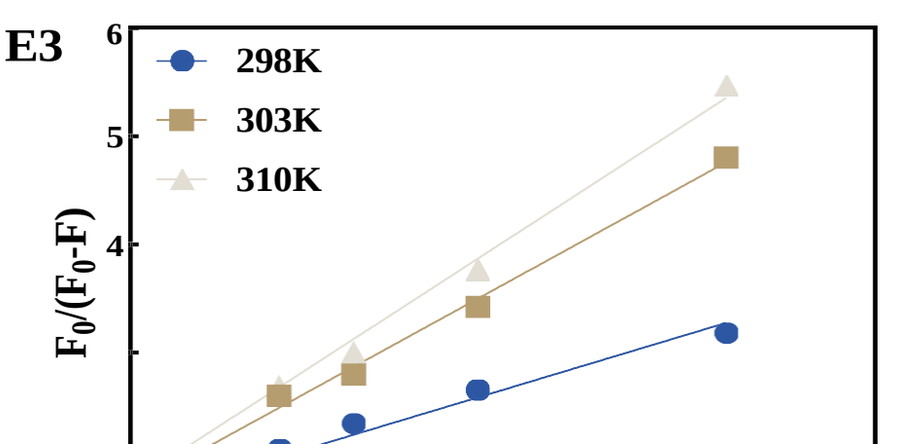

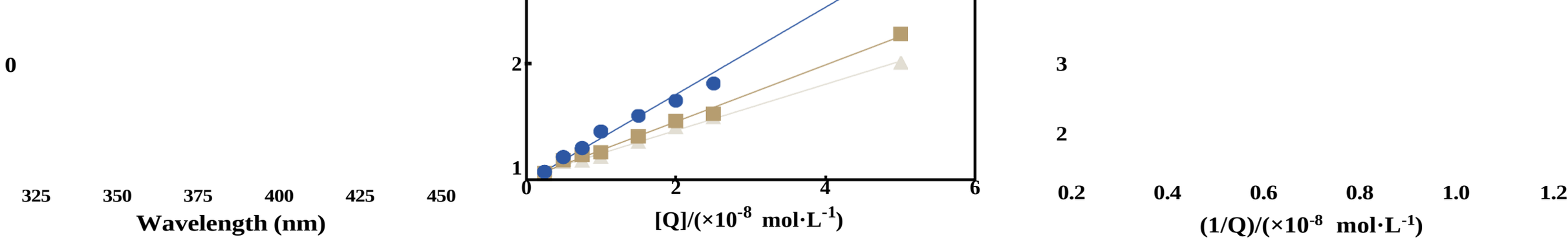
0
325
350
375
400
425
450
Wavelength (nm)
1
2
0
2
4
6
[Q]/(×10-8 mol·L-1)
2
3
0.2
0.4
0.6
0.8
1.0
1.2
(1/Q)/(×10-8 mol·L-1)

Figure 4

Click here to access/download;Figure;Figure 4.ppt

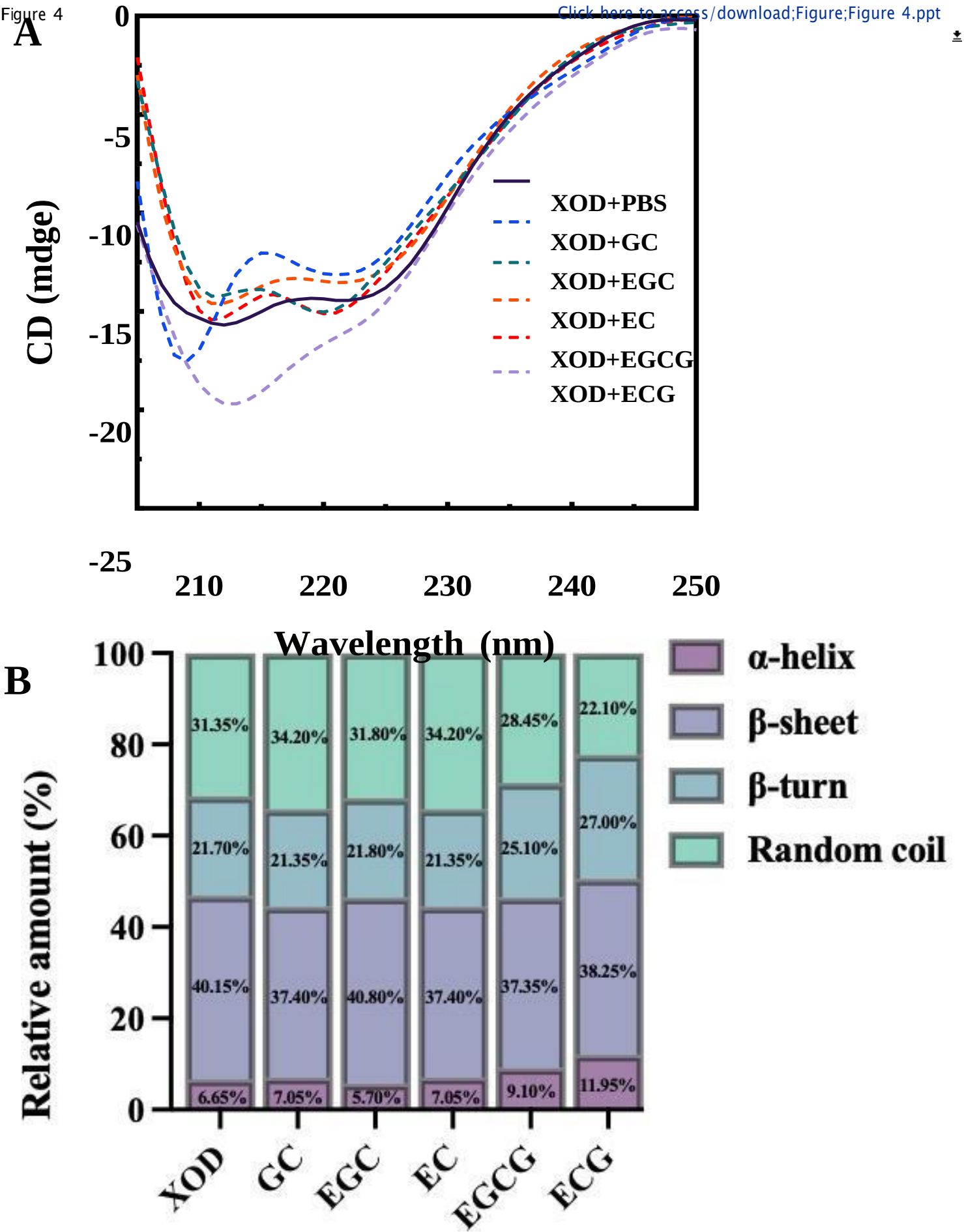

Figure 5

Click here to access/download;Figure;Figure 5.ppt

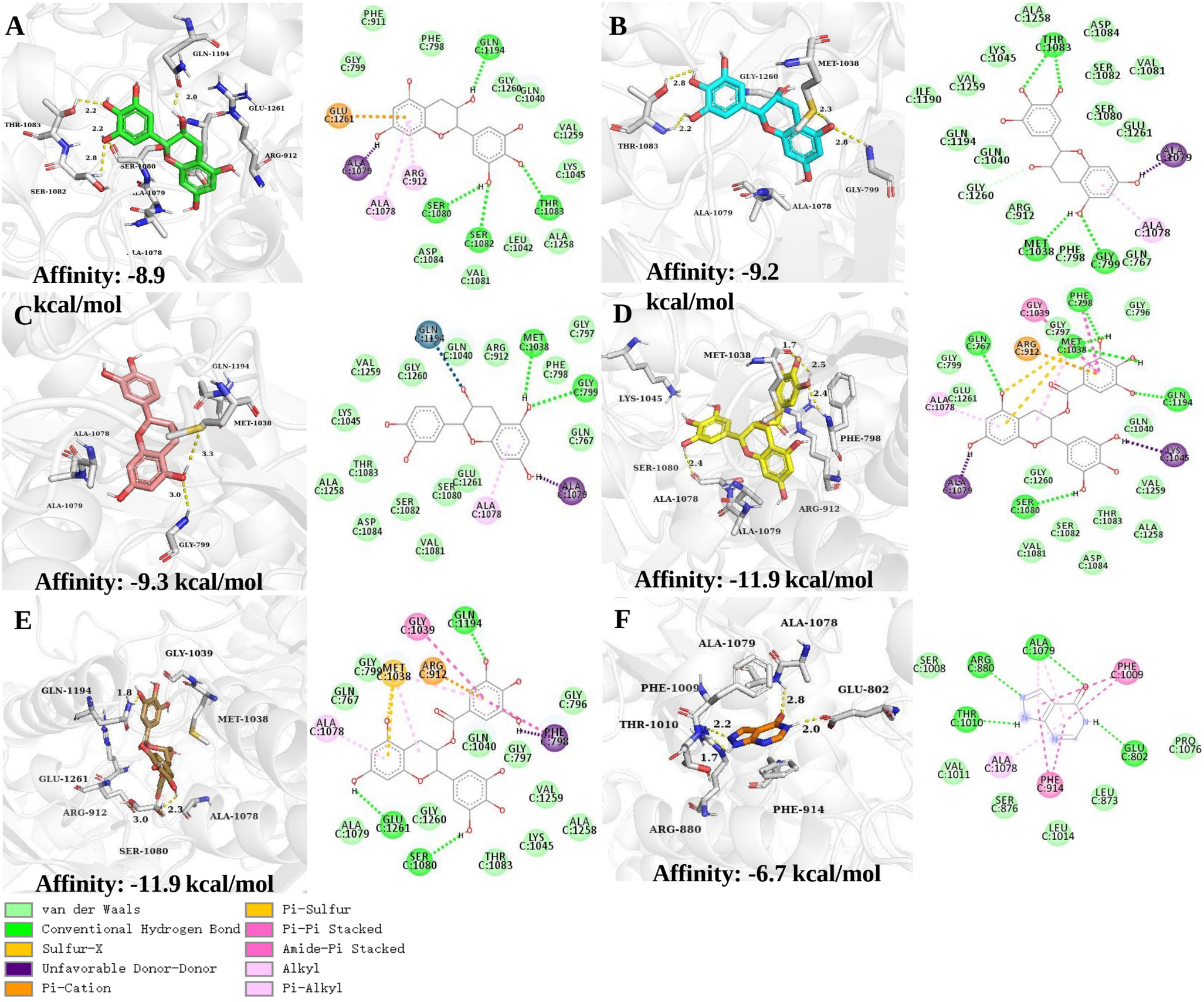

Figure 6

Click here to access/download;Figure;Figure 6.ppt

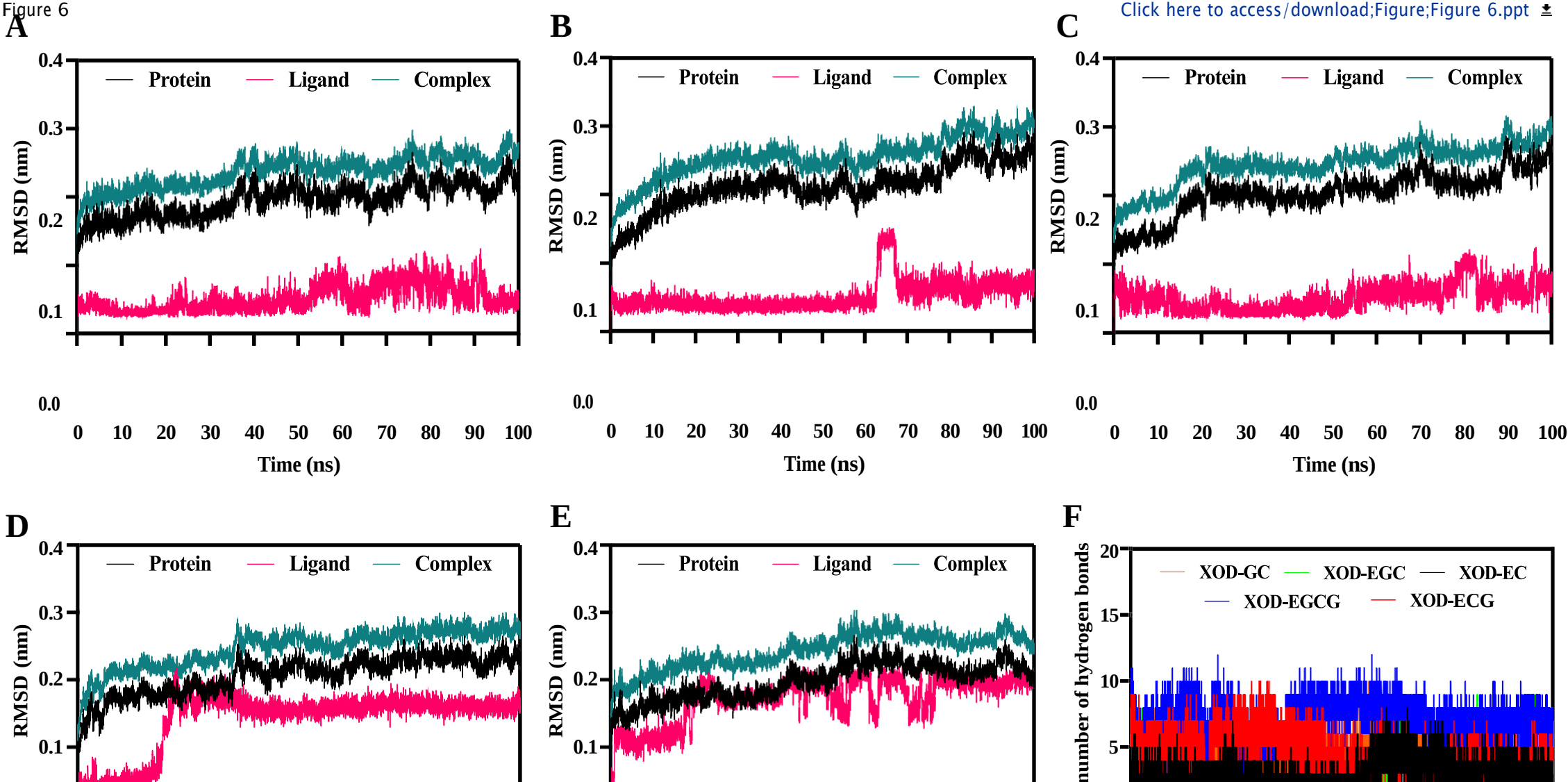

0.0
0 10 20 30 40 50 60 70 80 90 100
0.0
0 10 20 30 40 50 60 70 80 90 100
0
0 20 40 60 80 100
Time (ns)

Click here to access/download;Figure;Figure 7.ppt

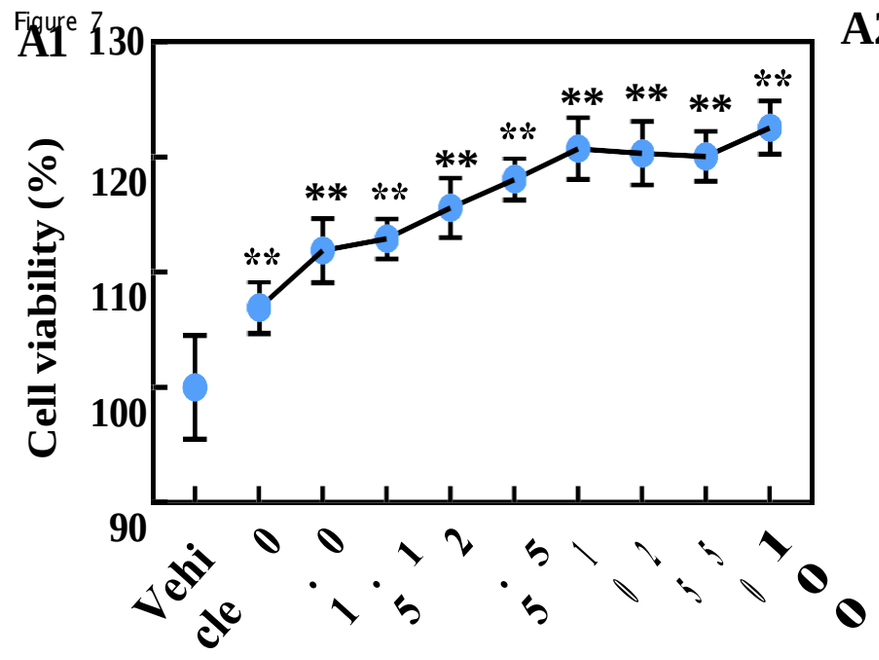

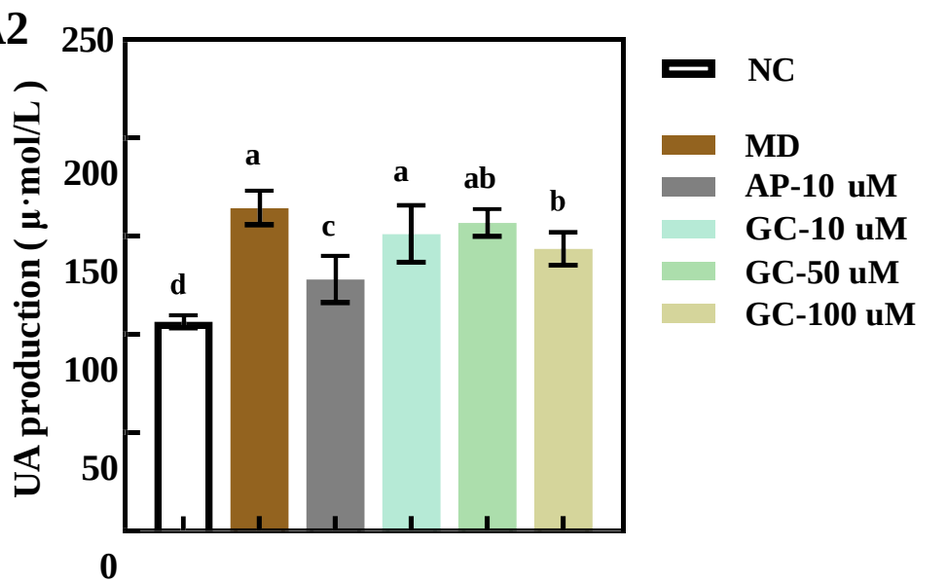

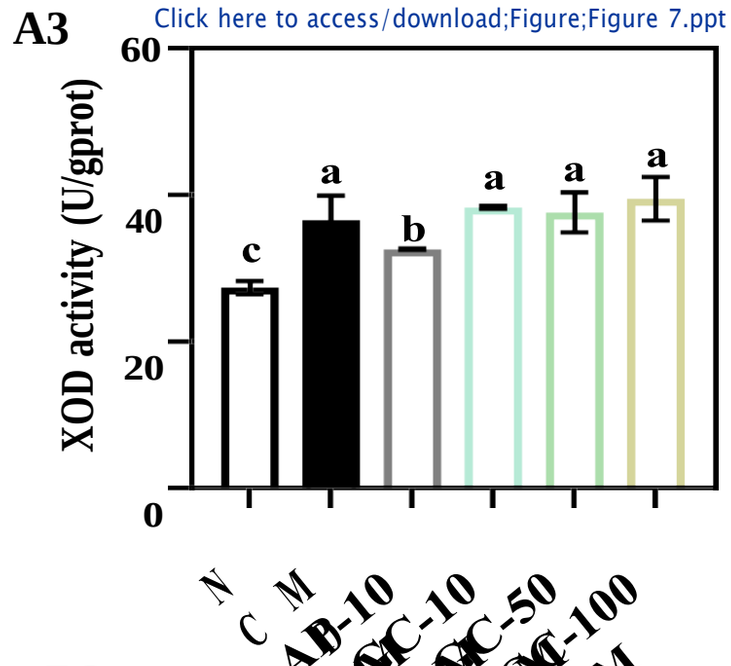

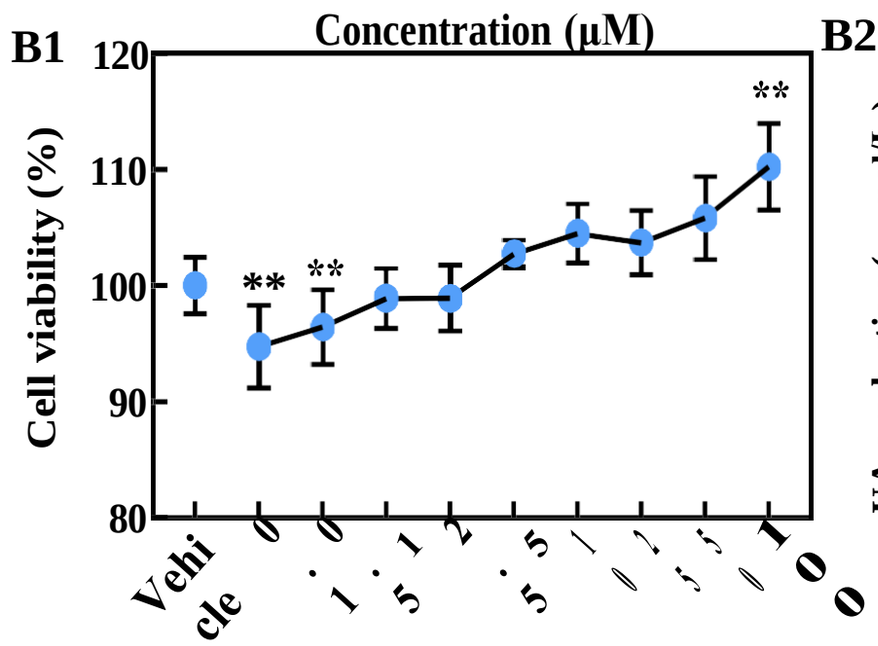

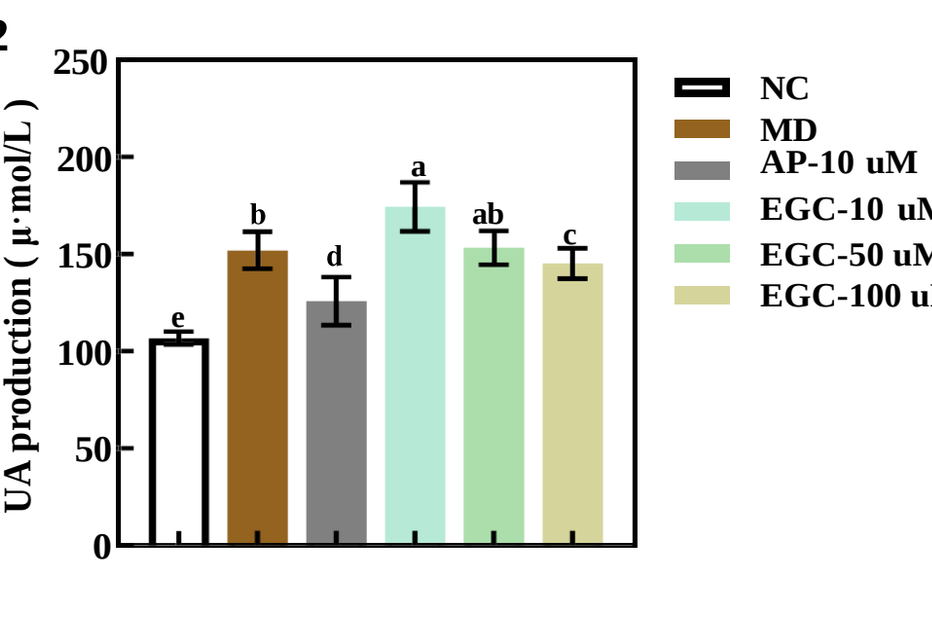

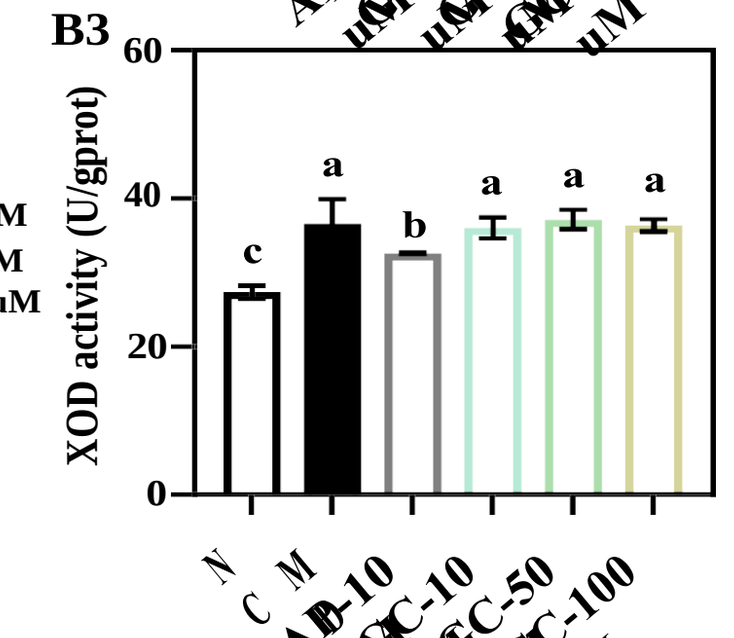

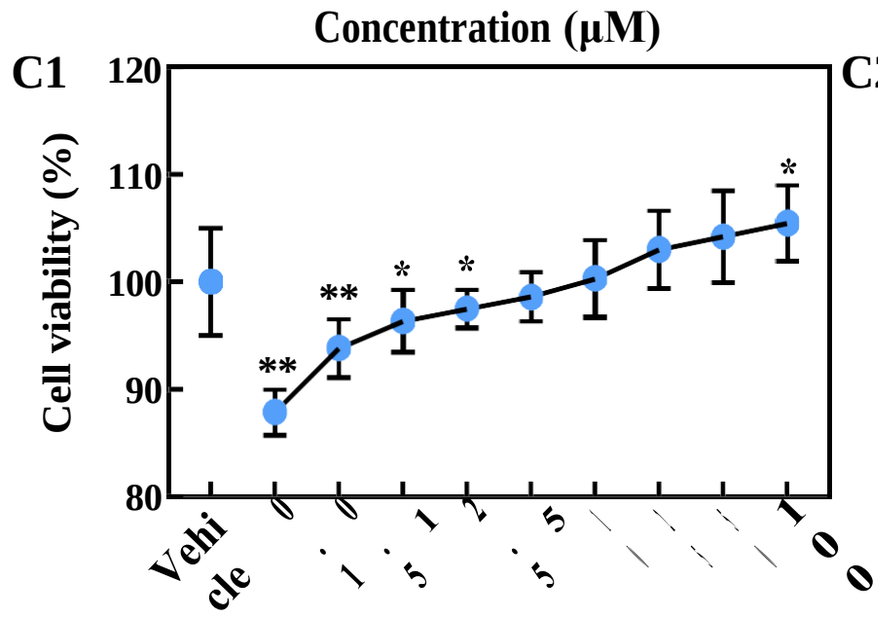

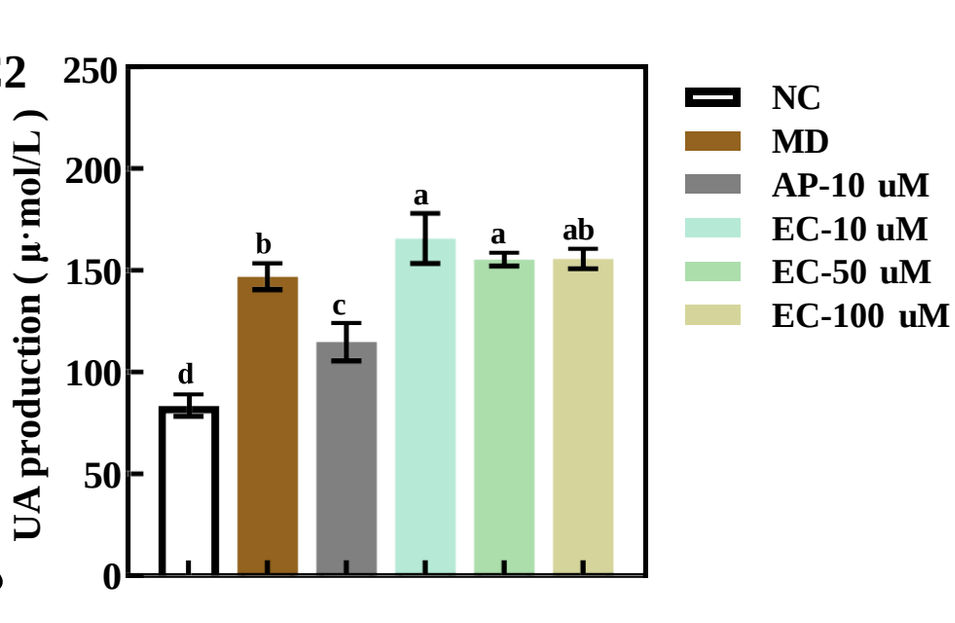

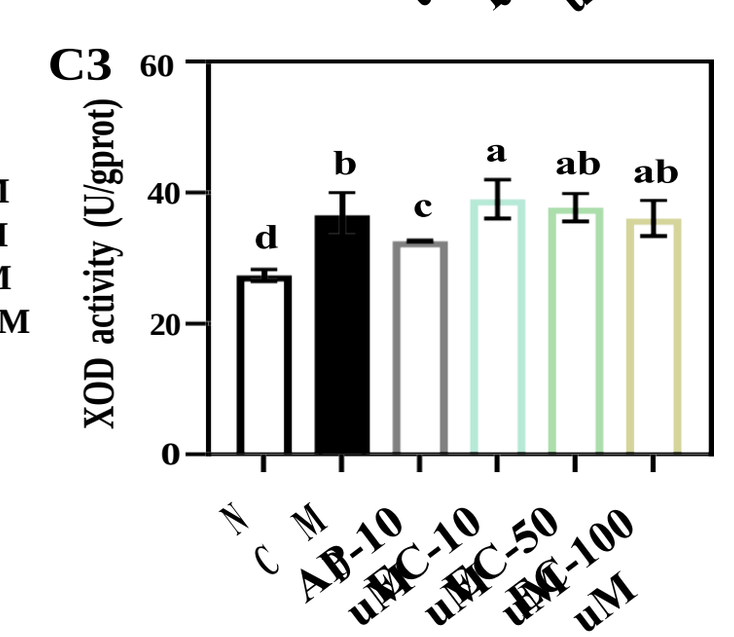

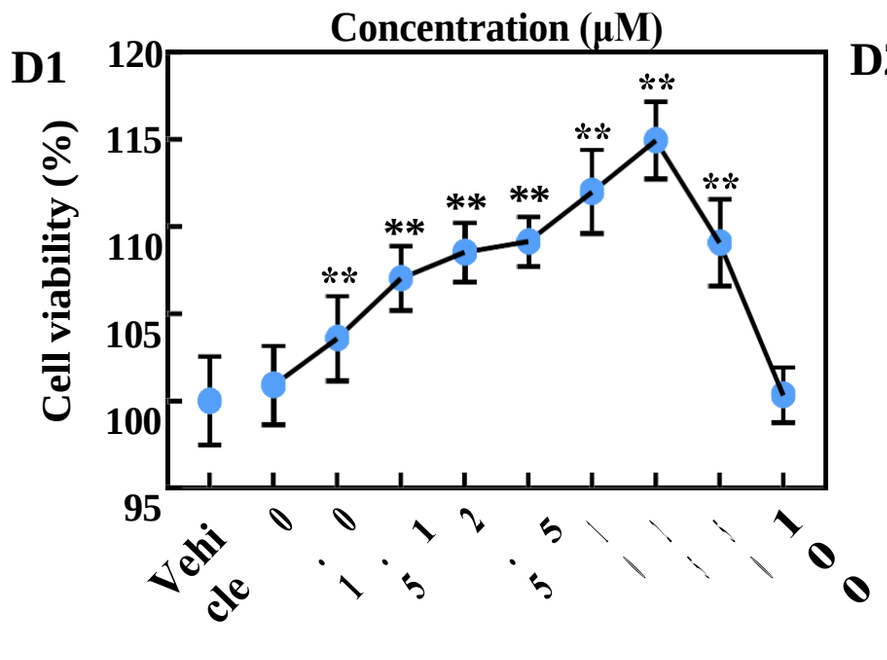

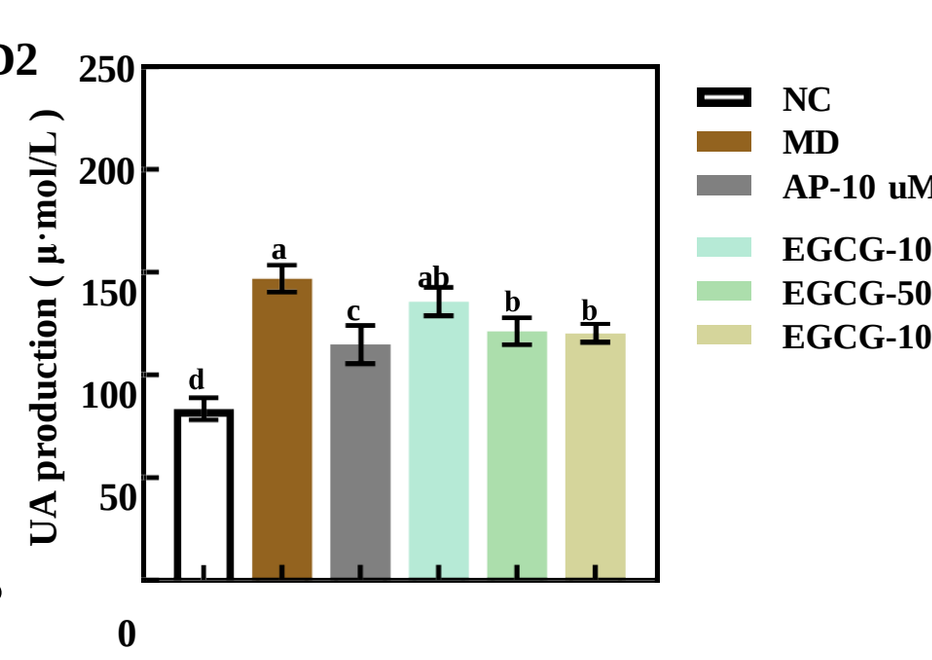

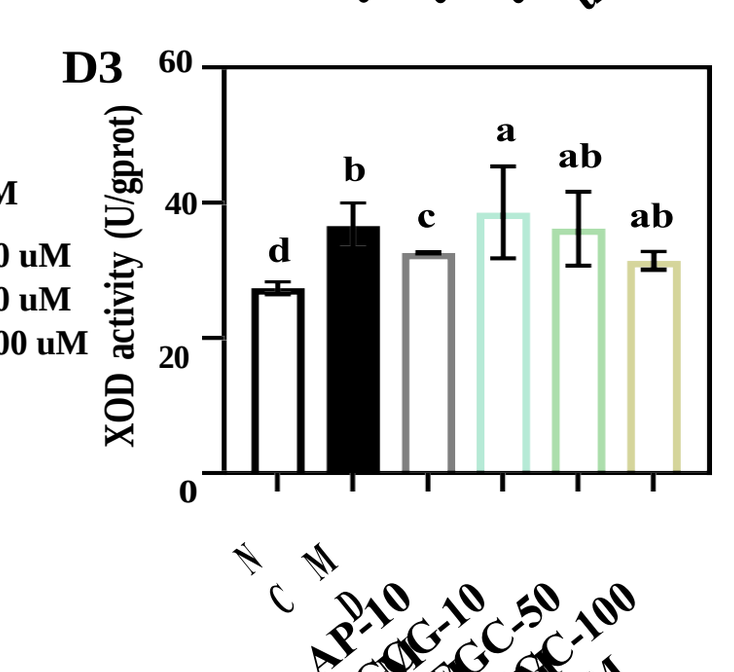

Concentration (μM)
100
0
AP-10
EMG-10
EMG-50
EMG-100
uM

Click here to access/download;Table (Editable version);Table 1.docx

Table 1

Inhibition kinetics parameters and types of five catechins to XOD

Systems	Concentrations (μM)	K_i (μM)	K_{is} (μM)	V_{max} (μM/min)	K_m (μM)	Inhibition types
XOD-GC	8	33.140	188.600	520.156	128.582	Mixed inhibition
	6			728.916	107.515	
	4			1021.763	81.638	
	2			1391.401	52.734	
	1			1764.602	58.231	
XOD-EGC	8	34.100	180.900	527.009	127.694	Mixed inhibition
	6			730.513	120.607	
	4			924.556	86.168	
	2			1314.233	45.866	
	1			1730.103	2.422	
XOD-EC	8	52.400	153.00	583.771	217.746	Mixed inhibition
	6			747.104	186.850	
	4			987.264	136.933	
	2			1353.363	64.961	
	1			1543.924	7.874	
XOD-EGCG	0.9	0.023	0.084	0.416	0.102	Mixed inhibition
	0.6			0.511	0.067	
	0.3			0.553	0.055	
	0.15			0.608	0.022	
	0.1			0.663	0.004	
XOD-ECG	0.9	0.028	0.070	0.437	0.097	Mixed inhibition
	0.6			0.524	0.060	
	0.3			0.563	0.045	
	0.15			0.608	0.025	
	0.1			0.645	0.009	

Click here to access/download;Table (Editable version);Table 2.docx

Table 2

Binding parameters of xanthine oxidase (XOD) with five catechins at three temperatures

Inhibitors	Temperature (K)	K_{sv} (10^4 L·mol^{-1})	R^2 1	K_q (10^{12} L·mol^{-1}·s^{-1})	K_a (10^4 L·mol^{-1})	R^2 2	n	R^2 3	ΔG (kJ·mol^{-1})	ΔH (kJ·mol^{-1})	ΔS (J·mol^{-1}·K^{-1})
GC	293K	0.5105	0.9964	0.5105	0.7506	0.9830	0.4266	0.8989	0.58416	-49.456	-0.16792
	303K	0.2702	0.9863	0.2702	0.5357	0.9907	0.5956	0.9642	1.42376		
	310K	0.1855	0.9718	0.1855	0.3228	0.9970	1.0863	0.9368	2.59920		
EGC	293K	0.5083	0.9945	0.5083	0.4029	0.9989	0.6090	0.9536	2.8716	-58.427	-0.20570
	303K	0.3649	0.9967	0.3649	0.3241	0.9963	0.5213	0.9624	3.9001		
	310K	0.2660	0.9948	0.2660	0.2618	0.9893	0.4659	0.9674	5.3400		
EC	293K	0.6252	0.9945	0.6252	0.6495	0.9980	0.3344	0.9859	1.0349	-19.840	-0.07005
	303K	0.4488	0.9967	0.4488	0.5740	0.9989	0.3798	0.9870	1.38515		
	310K	0.3272	0.9948	0.3272	0.4840	0.9997	0.4411	0.9884	1.8755		
EGCG	293K	1.2090	0.8813	1.2090	3.5505	0.8777	0.9448	0.9854	2.95544	-161.773	-0.55278
	303K	1.1540	0.9454	1.1540	2.0878	0.8561	0.8339	0.8917	5.71934		
	310K	1.0280	0.9414	1.0280	1.5950	0.9531	0.6042	0.9013	9.5888		
ECG	293K	4.1060	0.9923	4.1060	3.8099	0.9912	0.5757	0.9460	0.9095	-105.253	-0.35625
	303K	2.6720	0.9943	2.6720	2.2773	0.9500	0.6758	0.9611	2.69075		
	310K	2.1730	0.9941	2.1730	1.8472	0.8768	0.7273	0.9485	5.1845		

Graphical abstract

Multi-spectroscopy analysis

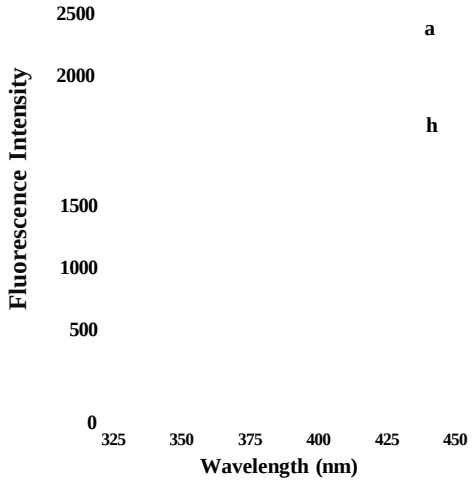

Molecular simulation

EGC

+

XOD

The inhibitory effect *in vitro* of XOD

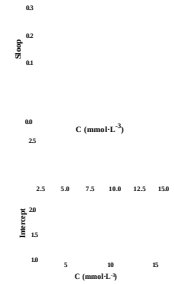

BRL-3a cell model

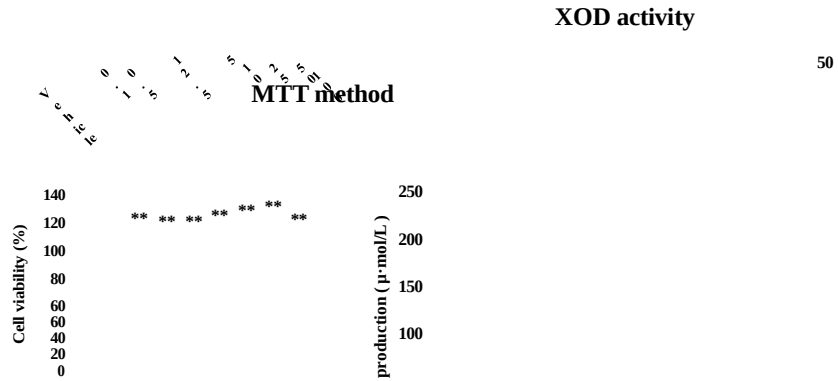

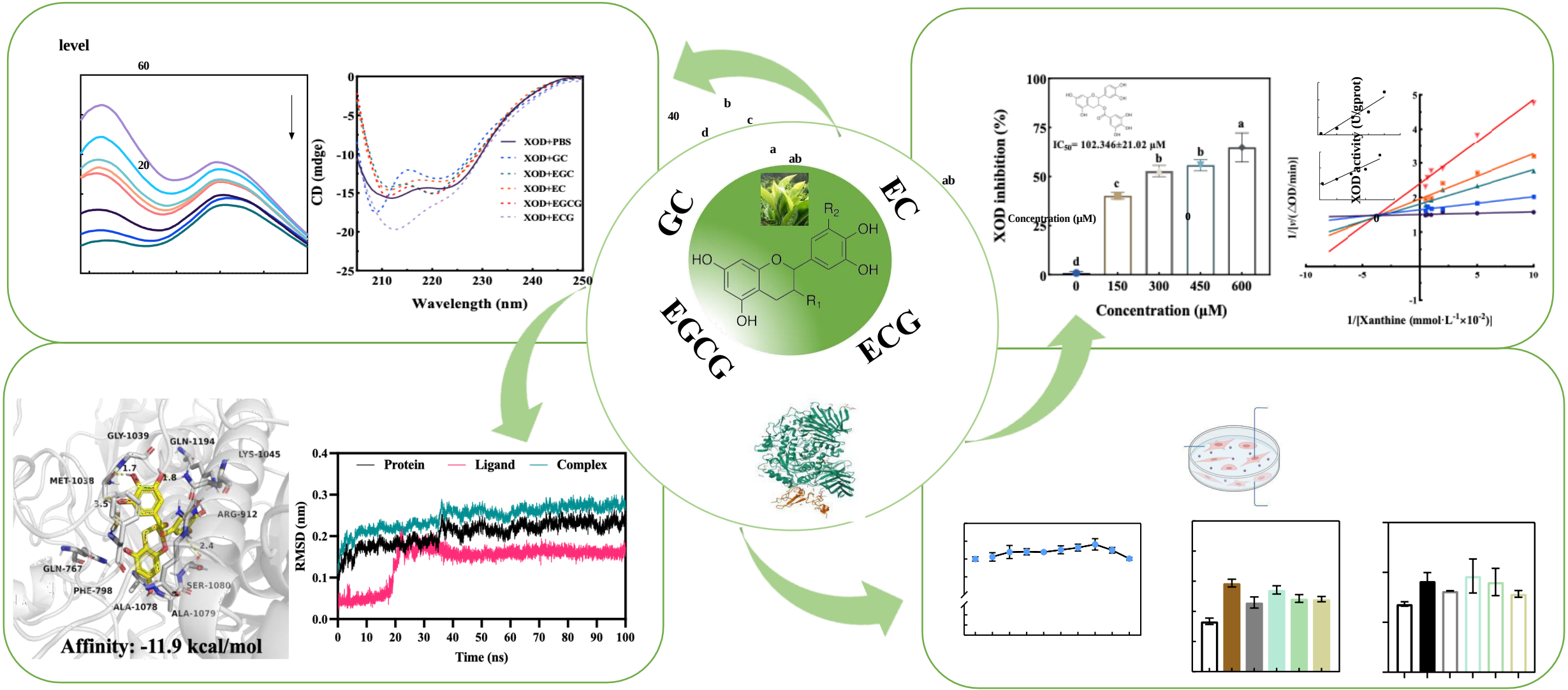
level
60
20
CD (mdge)
Wavelength (nm)
XOD+PBS
XOD+GC
XOD+EGC
XOD+EC
XOD+EGCG
XOD+ECG
GC
EC
EGCG
ECG
XOD inhibition (%)
Concentration (μM)
IC50= 102.346±21.02 μM
XOD activity (U/gprot)
1/[Xanthine (mmol·L-1×10-2)]
GLY-1039
GLN-1194
LYS-1045
MET-1038
ARG-912
GLN-767
PHE-798
SER-1080
ALA-1078
ALA-1079
Affinity: -11.9 kcal/mol
RMSD (nm)
Protein
Ligand
Complex
Time (ns)